

New Insights into the Complexation of Lead(II) by 1,4,7,10-Tetrakis(carbamoylmethyl)-1,4,7,10-tetraazacyclododecane (DOTAM): Structural, Thermodynamic, and Kinetic Studies

François Cuenot,^[a] Michel Meyer,^{*[a]} Enrique Espinosa,^{[a],[‡]} Arnaud Bucaille,^[a] Romain Burgat,^[a] Roger Guillard,^{*[a]} and Claire Marichal-Westrich^[b]

Keywords: Lead / Macrocyclic ligands / X-ray diffraction / NMR spectroscopy / Reaction mechanisms

The lead(II) coordination properties of the tetrapodal ligand DOTAM [1,4,7,10-tetrakis(carbamoylmethyl)-1,4,7,10-tetraaza-cyclododecane] have been investigated both in the solid state and in solution in order to ascertain the stereoactivity of the lone pair and to rationalize the structural effects of a cyclen-based scaffold on the metal uptake kinetics. The crystal structure of the free base shows that the pendant acetamide groups are not equivalent: two are folded over the macrocycle and maintained by an intramolecular hydrogen bond involving an amide hydrogen atom and a neighboring tertiary amine of the cyclen ring, while the other two are extended and point away from the macrocyclic cavity. The spontaneous reaction between Pb^{2+} and DOTAM, even under mild acidic conditions, leads to a mononuclear complex. The crystal structure of $[\text{Pb}(\text{DOTAM})](\text{NO}_3)_2 \cdot 3.5\text{H}_2\text{O}$ reveals that the eight-coordinate metal cation is trapped inside the

core of the ligand, interacting with the four cyclen nitrogen and the four amide oxygen atoms. The helical layout of the folded arms leaves no significant gap in the coordination sphere of Pb^{2+} , thus leading to a holodirected structure that is characteristic of a stereochemically inactive $6s^2$ electronic lone pair. While the coordination scheme is maintained in solution, variable temperature NMR studies enabled characterization of the dynamics related to the inversion of configuration of the amide substituents. Finally, the lead(II)-binding mechanism in aqueous solution has been investigated over a wide $\text{p}[\text{H}]$ range (1–7) by means of classical and stopped-flow spectrophotometry. The complexation reaction proceeds in a single rate-limiting step according to an Eigen–Winkler mechanism.

(© WILEY-VCH Verlag GmbH & Co. KGaA, 69451 Weinheim, Germany, 2008)

Introduction

For many years, efforts have been devoted towards the synthesis of highly specific sequestering agents for metal ion immobilization, extraction, or in vivo decorporation.^[1–3] Because of their toxicity, heavy metals are the principal targets of this research. Among them, lead is one of the most toxic elements and a widespread inorganic pollutant in the environment.^[4] Therefore, lead(II) is easily ingested by hu-

man beings through the gastrointestinal track, skin, or lungs. Once absorbed, it can cause many diseases and is particularly harmful to children.^[5,6] Among the various pathologies due to lead(II) poisoning, the most frequent is anemia. This disease results from the inhibition of δ -amino-levulinic acid dehydratase, a cytosolic zinc enzyme involved in the first step of heme biosynthesis, through the displacement of the Zn^{2+} -active site by a Pb^{2+} cation.^[5,7–9] Besides anemia, lead-induced enzymatic inhibition causes a range of other pathologies. One can quote, for example, the replacement of calcium by lead in synaptogamin^[5,10] or osteocalcin (bone Gla protein),^[11–13] which induces nervous system aftereffects or delays osseous growth, respectively.

From the viewpoint of either lead poisoning prevention and treatment, or remediation of contaminated liquids or environments, the design of highly specific lead(II)-chelating agents with respect to other relevant metal cations represents a real challenge. To reach that ultimate goal, the basic principles of chemical engineering provide some useful guidelines for a rational design of polydentate chelators that fulfill both the electronic and stereochemical requirements of the targeted species.^[14–20] Relying on the intermediate character of lead(II) in Pearson's HSAB classification,^[21–23] mixed ligands that combine soft (e.g., sulfur) or

[a] Institut de Chimie Moléculaire de l'Université de Bourgogne (ICMUB), UMR 5260 du CNRS, 9 avenue A. Savary, B. P. 47870, 21078 Dijon Cedex, France
Fax: +33-3-80396117
E-mail: Michel.Meyer@u-bourgogne.fr
Roger.Guillard@u-bourgogne.fr

[b] Ecole Nationale Supérieure de Chimie de Mulhouse (ENSCMu), Laboratoire de Matériaux à Porosité Contrôlée, UMR 7016 du CNRS, 3 rue A. Werner, 68093 Mulhouse Cedex, France

[‡] Current address: Laboratoire de Cristallographie et de Modélisation des Matériaux Minéraux et Biologiques (LCM3B), UMR 7036 du CNRS, Université Henri Poincaré Nancy 1, Faculté des Sciences et Techniques, boulevard des Aiguillettes, B. P. 239, 54506 Vandoeuvre-lès-Nancy Cedex, France

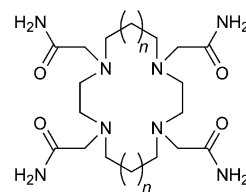
Supporting information for this article is available on the WWW under <http://www.eurjic.org/> or from the author.

intermediate bases (e.g., neutral carbonyl oxygen atoms) with a harder base like an amino nitrogen atom appear to be particularly adapted to sequester Pb^{2+} .^[21,24–26] This rationale is found behind all currently approved drugs used in chelation therapy for treating chronic lead overloads.^[27–31]

From a stereochemical point of view, the Pb^{2+} ion possesses an electronic lone pair ($6s^2$) that can be either stereochemically active, as a consequence of the hybridization of the $6s^2$ with the unoccupied $6p^0$ orbitals, or inactive according to the Valence Shell Electron Pair Repulsion (VSEPR) formalism.^[32] The activity of this electronic pair primarily depends on the nature and the number of the donor atoms bound to Pb^{2+} .^[33] For low coordination numbers ($n < 6$), the lone pair is active and exhibits a p character. Complexes featuring stereoactivity are characterized by (i) a hemidirected structure, (ii) lead–donor atom bond lengths generally shorter than 2.6 Å when the donor is opposite to the gap found in the coordination sphere, (iii) a more covalent character of the interaction, (iv) only very weak interactions of the lone pair with its environment, and (v) a contraction of the ionic radius of the Pb^{2+} ion.^[34,35] In contrast, inactivity of the $6s^2$ lone pair results in a holodirected arrangement of the donor atoms around the metal center and is usually found for lead(II) complexes with high coordination numbers ($n > 8$). In the case of hexa-, hepta-, or octacoordinate lead(II) complexes, the prediction is less reliable, as both types of arrangement can be observed depending on the nature of the ligand.^[6]

Cyclic and open-chain polyamines are well known to be good chelating agents of divalent heavy metals and lead(II) in particular.^[1,36–40] Derivatization of the primary or secondary nitrogen atoms by appending coordinating groups^[41] is a further means to fine-tune both the affinity and selectivity. In 1995, Maumela et al.^[42] reported the astonishing stability of the cadmium(II) and lead(II) complexes formed with DOTAM, the N,N',N'',N''' -tetraacetamide derivative of cyclen (Scheme 1, $n = 0$), as they retain their integrity even under strongly acidic conditions (e.g., 0.5 M HCl). Thus, only a lower limit for the binding constant has been estimated from competitive titration experiments ($\log \beta_{110} > 19$; $I = 0.1$ M; $T = 298$ K). The extreme binding affinity of DOTAM contrasts with that observed for the cyclam-based analog TETAM (Scheme 1, $n = 1$), as the corresponding lead(II) complex is destabilized by more than 10 orders of magnitude upon enlarging the ring size from 12 to 14 atoms.^[15] As a consequence, the latter ligand was considered as an easily regenerable extracting agent for lead removal from tap water by grafting the macrocycle onto the surface of silica gel.^[14,43]

Recently, Hancock et al. described the crystal structure of the $[\text{Pb}(\text{DOTAM})](\text{ClO}_4)_2 \cdot 4.5\text{H}_2\text{O}$ complex, in which a water molecule is vertically aligned with the metal center at a $\text{Pb} \cdots \text{O}$ distance of 3.52 Å.^[44] The authors concluded that the electronic lone pair is stereochemically active and orientated in such a way that it might allow a weak interaction between one water hydrogen atom and the lead center, although they ruled out the possibility of hydrogen bond formation.



Scheme 1. $n = 0$: DOTAM; $n = 1$: TETAM.

In order to clarify this situation and to get a deeper insight into the lead(II) coordination chemistry of DOTAM, we present herein the crystal structures of the free ligand and of the complex obtained with lead nitrate, $[\text{Pb}(\text{DOTAM})](\text{NO}_3)_2 \cdot 3.5\text{H}_2\text{O}$. A detailed analysis of the coordination polyhedron provides new evidence for the stereochemical inactivity of the $6s^2$ lone pair. Structural properties were further explored by means of multinuclear (^1H , ^{13}C , and ^{207}Pb) NMR spectroscopy both in the solid state and in solution. The configuration inversion mechanism of the $[\text{Pb}(\text{DOTAM})]^{2+}$ cation, which exists as a racemic mixture of two enantiomers, was probed by variable-temperature NMR studies. Finally, the complexation kinetics of Pb^{2+} by DOTAM in aqueous solution is presented. The reaction rates measured by classical or stopped-flow absorption spectrophotometry are compared to the previously published values pertaining to the cyclam-based analog TETAM.^[15]

Results and Discussion

X-ray Crystal Structure and CPMAS NMR Studies of DOTAM

Although the X-ray crystal structure of unprotonated DOTAM has been disclosed by Lloyd and Luckay in a short note,^[45] we provide herein a more detailed description. Relevant crystal data and refinement details are given in the Experimental Section. DOTAM crystallizes free of water as colorless prisms in the monoclinic $P2_1/c$ space group with two molecular units per unit cell. The structure consists of discrete centrosymmetric molecules; hence the asymmetric unit corresponds to a half molecular unit. An ORTEP view of the molecule with the atomic labeling scheme is shown in Figure 1. An exhaustive listing of bond lengths and angles has been deposited as Supporting Information. Average $\text{C}(\text{sp}^3)\text{--N}$ [1.469(9) Å], $\text{C}(\text{sp}^2)\text{--NH}_2$ [1.338(6) Å], and $\text{C}(\text{sp}^2)\text{--O}$ [1.234(4) Å] distances are typical for tertiary amines^[46,47] and primary amides,^[48] respectively.

Intramolecular hydrogen bonds between the amide protons H131 and H131', and the neighboring tertiary amines N2 and N2' [$\text{H131} \cdots \text{N2} = 2.17(2)$ Å, $\text{N13} \cdots \text{N2} = 3.023(2)$ Å, $\text{N13--H131} \cdots \text{N2} = 156.2(2)^\circ$] are responsible for the folding over of the macrocyclic cavity of the acetamide groups borne by N1 and N1', one above and the other below the mean ring plane. Furthermore, these hydrogen-bonding interactions have a significant effect on the conformation of each equivalent acetamide group, as they enforce

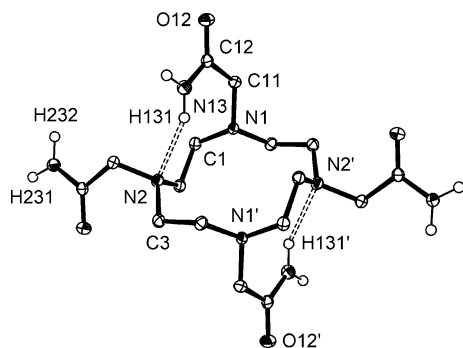


Figure 1. ORTEP view of the deprotonated ligand DOTAM. Ellipsoids are at the 50% probability level. Nonrelevant hydrogen atoms have been omitted for clarity.

an almost planar arrangement of the entire arm. Deviations from the least-squares mean plane are: 0.005(1) (N1), $-0.008(1)$ (C11), 0.004(1) (C12), 0.002(1) (O12), and $-0.004(1)$ Å (N13) with a root mean square deviation (rmsd) of 0.0048 Å. The planarity is also reflected by the values of the relevant N1–C11–C12–N13 and N1–C11–C12–O12 torsion angles, 1.3(2) and $-179.6(1)^\circ$, respectively.

Conversely, the two opposite acetamide chains appended to N2 and N2' are extended and point away from the cycle. They form an intermolecular hydrogen-bond network involving both amide hydrogen atoms and the oxygen atoms of two different adjacent molecules [$\text{H231}\cdots\text{O12} = 2.01(2)$ Å, $\text{N23}\cdots\text{O12} = 2.899(2)$ Å, $\text{N23}\cdots\text{H231}\cdots\text{O12} = 176.4(2)^\circ$; $\text{H232}\cdots\text{O22} = 2.16(2)$ Å, $\text{N23}\cdots\text{O22} = 3.015(2)$ Å, $\text{N23}\cdots\text{H232}\cdots\text{O22} = 160.1(2)^\circ$]. Although this set of side chains is also planar [rmsd = 0.0032 Å; the individual deviations from the least-squares plane are: $-0.0016(4)$ (C21), 0.006(1) (C22), $-0.0022(5)$ (O22), and $-0.0018(4)$ Å (N23)], the intermolecular interactions maintain them tilted with respect to the 12-membered ring, as evidenced by the values of the N2–C21–C22–N23 [$-151.3(1)^\circ$] and N2–C21–C22–O22 [$29.8(2)^\circ$] dihedral angles and by the large deviation of the N2 atom [0.630(3) Å] that was not included in the mean plane calculation.

In the case of the cyclam analog TETAM, the four macrocyclic nitrogen atoms are hydrogen-bonded to amide hydrogen atoms, the four amide substituents being folded on the top of the cyclam ring.^[15] As both DOTAM and TETAM possess four identical acetamide groups, the stereochemical differences between these ligands can only arise from the tethering effect imposed by the semi-rigid tetraaza-macrocyclic scaffold. The 12-membered ring of DOTAM enforces higher constraints than the more flexible 14-membered skeleton of TETAM. These constraints do not only affect the number of intramolecular bonds, but also the atoms involved in these weak interactions.

The macrocyclic ring conformation is most adequately described in terms of torsion angle sequences according to the definition of corners and pseudocorners introduced by Dale.^[49,50] Assigning τ_1 to the N1–C1–C2–N2 torsion angle, the following sequence for τ_1 – τ_6 is found: 74, -153.4 , 87.9, -80.3 , 159.2, and -92.4° . Thus, the cyclen ring displays

a quasitetragonal shape delimited by two genuine (C1 and C1') and two pseudocorners (C3 and C3'), the C1 \cdots C3 (3.759 Å) and C1 \cdots C3' (3.780 Å) edges being almost perpendicular to each other (C1 \cdots C3 \cdots C1' = 84.1° and C3 \cdots C1 \cdots C3' = 95.9°). In order to distinguish the different stereoisomers, which may arise when the macrocycle contains heteroatoms at different relative locations, we have extended Dale's nomenclature by adding a capital letter to the series of digits corresponding to the number of chemical bonds counted between two genuine corners.^[46] Accordingly, the ring takes a [6,6]-B conformation where each nitrogen atom is located one bond away from a vertex.

Alternatively, the same arrangement might be classified as a type III structure following the widely used stereochemical classification proposed by Bosnich et al.,^[51] which relies entirely on the directionality (i.e., chirality) of the four exocyclic N–R bonds with respect to the four-nitrogen-atom plane (N₄). As previously pointed out,^[52] there is a direct correspondence between the formalisms of Dale and Bosnich, although the latter neglects a priori the three-dimensional layout of the ethylenediamine fragments connecting the four amine nitrogen atoms. Indeed, their chirality is unique and imposed by the overall ring conformation when the amine is not occupying a corner or pseudocorner position. Thus, tetrasubstituted cycloalkanes displaying a centrosymmetric [6,6]-B ring conformation like DOTAM are constrained to adopt a type III configuration for which one pair of adjacent *N*-substituents is oriented above the mean macrocyclic plane and the other pair below. Conversely, the [3,3,3,3]-B arrangement observed for the parent tetraamine cyclen^[53] enforces all four substituents to point towards the same side of the plane (Bosnich's type I configuration), thus preorienting the appended groups in a more favorable position to bind a metal ion.^[54,55]

The solid-state structure of powdered DOTAM was further investigated at room temperature by CPMAS NMR spectroscopy. In agreement with the symmetry found in the crystal structure, the ^{15}N CPMAS NMR spectrum exhibits four resonances that divide into two sets. The first one corresponds to the nonequivalent tertiary amines (-340.6 and -343.7 ppm), while the second pair of lines is assigned to the amide nitrogen atoms (-270.8 and -272.3 ppm). The ^{13}C CPMAS NMR spectrum shows five resonances between $\delta = 53.5$ and 62.5 ppm but the intensity of the peak at $\delta = 55.8$ ppm is twice that of the others. These lines are easily attributed to the nonequivalent methylene carbon atoms belonging to the 12-membered cyclen ring and acetamide dangling side chains. It is worth noting that each CH_2 resonance features a shoulder with approximate 1:2 intensity ratio due to a heteronuclear dipolar interaction between the ^{14}N and ^{13}C nuclei that is not completely averaged out by magic angle spinning.^[56] Two doublets are also observed between 175.5 and 177.3 ppm, which correspond to both nonequivalent carbonyl groups as predicted by the structure. The splitting of both lines with an apparent 1:1 intensity ratio may also be due to the dipolar interaction between the ^{13}C and ^{14}N nuclei of the neighboring NH_2 groups, as already observed for various nitroanilines.^[57]

Synthesis, Spectroscopic Characterization, and X-ray Crystal Structure of $[\text{Pb}(\text{DOTAM})](\text{NO}_3)_2 \cdot 3.5\text{H}_2\text{O}$

Slow evaporation at room temperature of an equimolar amount of DOTAM and $\text{Pb}(\text{NO}_3)_2$ in a methanol/water mixture (10:1 v/v) afforded colorless crystals of $[\text{Pb}(\text{DOTAM})](\text{NO}_3)_2 \cdot 3.5\text{H}_2\text{O}$. MALDI-TOF mass measurements revealed the molecular ion peak with the correct isotope pattern together with signals assigned to the free ligand and its adducts with sodium and potassium. Laser-induced demetalation during the desorption process is a typical behavior for this type of compound.^[15] Infrared spectroscopy provided structural evidence for the binding of the carbonyl oxygen atoms to Pb^{2+} , as bond strength weakening upon complexation results in a 30 cm^{-1} bathochromic shift of the carbonyl stretching mode.

The crystal structure was solved in the same space group as the deprotonated ligand ($P2_1/c$), but revealed some degree of disorder associated with both counteranions and some cocrystallized water molecules (Table 7). Thus, both NO_3^- anions in the asymmetric unit are disordered between two positions exhibiting site occupation factors (sof) of 0.70:0.30 and 0.50:0.50, respectively. This arrangement is related to the disorder observed for two water molecules. While one of the water molecules shares in a complementary way both positions taken by one nitrate anion (sof of 0.30:0.70), the second one is located also on a position left vacant by the second nitrate anion, although only one of the two possible sites is occupied (sof of 0 and 0.5, respectively). Thus, along with two ordered water molecules, a total of 3.5 water molecules are cocrystallized per complex. The fast degradation of the crystals when they are kept in air at room temperature is probably related to the above-mentioned disorder. Indeed, the holes created in the crystal lattice by the missing water molecule in one over two unit-cells, together with the introduction of smaller molecules (H_2O) in some of the positions otherwise occupied by the bulkier NO_3^- anions, are responsible for a weakening of the cohesive forces and might explain the high desolvation propensity of the crystals.

An ORTEP drawing of the octacoordinate lead complex is shown in Figure 2, while a selection of relevant bond lengths and angles is summarized in Table 1. As expected,

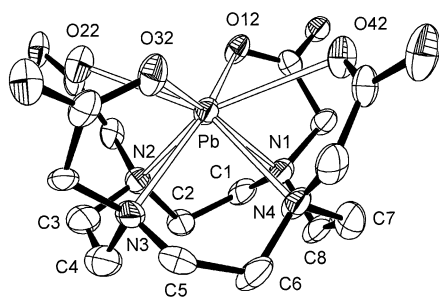


Figure 2. ORTEP view of the $[\text{Pb}(\text{DOTAM})]^{2+}$ complex in the crystal structure of $[\text{Pb}(\text{DOTAM})](\text{NO}_3)_2 \cdot 3.5\text{H}_2\text{O}$. Ellipsoids are drawn at the 50% probability level. Hydrogen atoms have been omitted for clarity.

the strength of the carbonyl double bonds is weakened upon binding to lead [$\text{C}-\text{O}_{\text{av}} = 1.25(1)$ vs. $1.234(4)\text{ \AA}$ for the complex vs. the free ligand], in agreement with a shift of about 30 cm^{-1} to lower wavenumbers of the corresponding infrared stretching mode. Concomitantly, the sp^2 character (i.e., the π conjugation) of the amide nitrogen atoms is significantly enhanced, as evidenced by the shortening of the average $\text{C}(\text{sp}^2)-\text{NH}_2$ bond length in the complex [$1.31(1)$ vs. $1.338(6)\text{ \AA}$]. The $\text{Pb}-\text{N}$ distances are fairly regular and average $2.625(6)\text{ \AA}$, whereas the oxygen atoms give rise to a larger dispersion in bond lengths with a mean $\text{Pb}-\text{O}$ distance of $2.75(7)\text{ \AA}$. A close examination of the metric data collected in Table 1 reveals the formation of two pairs of alternating shorter [$2.71(7)\text{ \AA}$] and longer [$2.80(2)\text{ \AA}$] $\text{Pb}-\text{O}$ bonds, located *trans* to each other, involving O12 and O32 for the former, and O22 and O42 for the latter.

Table 1. Selected bond lengths and angles in the complex $[\text{Pb}(\text{DOTAM})](\text{NO}_3)_2 \cdot 3.5\text{H}_2\text{O}$.

Bond lengths [\AA]		Bond angles [$^\circ$]	
Pb–N1	2.617(8)	N1–Pb–N2	69.4(3)
Pb–N2	2.625(9)	N2–Pb–N3	70.2(3)
Pb–N3	2.628(8)	N3–Pb–N4	69.1(3)
Pb–N4	2.630(9)	N4–Pb–N1	69.3(3)
Pb–O12	2.657(6)	O12–Pb–O22	80.9(2)
Pb–O22	2.785(5)	O22–Pb–O32	82.8(2)
Pb–O32	2.756(6)	O32–Pb–O42	84.4(2)
Pb–O42	2.819(5)	O42–Pb–O12	83.7(2)

The ORTEP side view displayed in Figure 2 evidences the structural rearrangement undergone by the ligand upon metal binding. The Pb^{2+} ion is bound to the four macrocyclic amine nitrogen atoms and to the four amide oxygen atoms provided by the side chains, which project towards the same face of the capping ring. To achieve this four-branched sugar-tong-type architecture, which is classical for cyclen derivatives bearing chelating groups,^[46,58,59] the macrocycle switches from a [6,6]-B to a [3,3,3,3]-B conformation where C1, C3, C5, and C7 define the corner positions. The lateral chains adopt a chiral right- (Δ) or left-handed (Λ) four-blade propeller-like layout, which in turn imposes the same puckered conformation to each of the four five-membered chelate rings belonging to the macrocycle, introducing an additional element of chirality. According to Corey and Bailar's nomenclature, which relies on the sign of the $\text{N}-\text{C}-\text{C}-\text{N}$ dihedral angles (δ for a positive and λ for a negative sign),^[60] the tetraazamacrocyclic moiety may occur either as the clockwise ($\delta,\delta,\delta,\delta$) or anti-clockwise ($\lambda,\lambda,\lambda,\lambda$) enantiomeric form. Analysis of the coordination polyhedron indicates that the crystal lattice contains pairs of discrete Δ -($\delta,\delta,\delta,\delta$) and Λ -($\lambda,\lambda,\lambda,\lambda$) $[\text{Pb}(\text{DOTAM})]^{2+}$ enantiomers, as evidenced by the average values of the $\text{N}-\text{C}-\text{C}-\text{N}$ [$58.8(6)^\circ$] and $\text{N}-\text{C}-\text{C}-\text{O}$ [$21(1)^\circ$] torsion angles. Hence, the homochiral stereochemistry around the central lead cation is best described as a distorted inversed or twisted square antiprism (TSAP) of approximate C_4 symmetry (Figure 3).

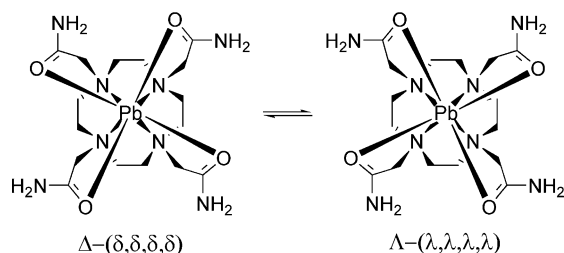


Figure 3. Schematic representation viewed down the C_4 axis of the two $\Delta-(\delta,\delta,\delta,\delta)$ and $\Lambda-(\lambda,\lambda,\lambda,\lambda)$ enantiomeric forms of the $[\text{Pb}(\text{DOTAM})]^{2+}$ complex.

The four nitrogen and four oxygen atoms form a set of two quasiparallel planes ($\omega = 0.42^\circ$) twisted by an average angle of $\phi = 26(1)^\circ$ along the pseudo C_4 axis and characterized by a $\text{Ct}_\text{N} \cdots \text{Ct}_\text{O}$ distance of 2.518 Å (Figure 4). The nitrogen atoms deviate by no more than 0.0009 Å from the N_4 mean plane, whereas the planar arrangement of the oxygen atoms is somewhat less regular, having deviations attaining ± 0.01 Å. In spite of the significantly longer Pb–O distances, the lead center is located closer to the plane defined by the oxygen than by the nitrogen atoms ($\text{Pb} \cdots \text{O}_4 = 0.964$ Å vs. $\text{Pb} \cdots \text{N}_4 = 1.554$ Å) and sits only 0.008 Å away from the line joining both Ct_N and Ct_O centroids. It follows that the eight donor atoms in the $[\text{Pb}(\text{DOTAM})](\text{NO}_3)_2 \cdot 3.5\text{H}_2\text{O}$ complex occupy two opposite calottes of a hypothetical sphere centered on the Pb^{2+} cation. This arrangement, combined with the typical and regular Pb–N and Pb–O bond lengths, strongly suggests a holodirected structure with a stereochemically inactive $6s^2$ lone pair.^[33]

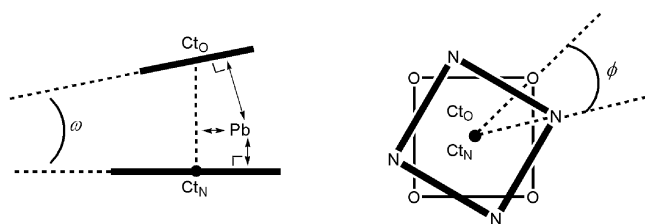


Figure 4. Structural parameters used to describe the coordination polyhedron of $[\text{M}(\text{DOTAM})]^{2+}$ complexes. Ct_N and Ct_O stand for the centroid of the four nitrogen and oxygen atoms, respectively.

In 2004, Hancock et al. reported the crystal structure of the $[\text{Pb}(\text{DOTAM})](\text{ClO}_4)_2 \cdot 4.5\text{H}_2\text{O}$ complex, which contains two independent but similar $[\text{Pb}(\text{DOTAM})]^{2+}$ cations.^[44] One has a water molecule placed 3.52 Å away from the lead center above the mean O_4 plane, while in the other there is an amide nitrogen atom in the same position at a distance of 4.1 Å. Based on these observations and on the presence of a small gap in the oxygen coordination calotte, they concluded that the lone pair is stereoactive and located on the $\text{Pb}-\text{O}_\text{water}$ or $\text{Pb}-\text{N}_\text{amide}$ fourfold symmetry axis. However, it can be argued that hydrogen atoms belonging to the water molecule could not be localized in the Fourier map and thus they were placed at calculated positions, the closest being approximately 3.3 Å away from the Pb^{2+} cation. The authors considered several possible orientations of these hydrogen atoms and for all of them they concluded that one

proton was held in the vicinity of the lead center by means of an agostic interaction, even if it was not directly pointing to it, thus supporting the stereoactivity of the lone pair.

Moreover, superposition of the crystal structure presented herein with those solved by Hancock et al. shows that the $[\text{Pb}(\text{DOTAM})]^{2+}$ cations are essentially identical (Figure 5), the root mean square deviation calculated by the Chem3D software between non-hydrogen atoms being equal to 0.17 and 0.11 Å. Remarkably, the major differences are only seen for the carbon atoms, while the N_4O_4 donor sets overlay almost perfectly. This is a clear indication that the occurrence of an exogenous water molecule or an amide nitrogen atom along the fourfold rotation axis has no influence on the positioning of the carbamoyl oxygen centers and therefore their presence cannot be viewed as a criterion to assess the activity of the lone pair. In addition, typical Pb–O and Pb–N distances for inactive lead compounds are observed for both nitrato and perchlorato species, whereas an active lone pair requires shorter Pb–L distances in the hemisphere opposite to the lone pair, where L stands for any donor atom.

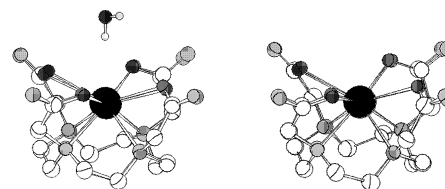
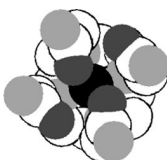
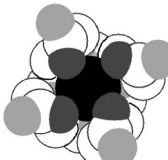
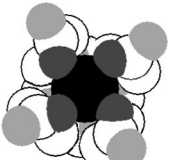
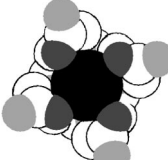


Figure 5. Chem3D overlays of the lead(II) complexes from $[\text{Pb}(\text{DOTAM})](\text{NO}_3)_2 \cdot 3.5\text{H}_2\text{O}$ (this work) and $[\text{Pb}(\text{DOTAM})](\text{ClO}_4)_2 \cdot 4.5\text{H}_2\text{O}$ obtained by Hancock et al.^[44]

In our view, the small gap in the coordination sphere of the Pb^{2+} ion is more likely explained in terms of van der Waals contacts and steric repulsion between oxygen atoms rather than electronic properties of the $6s^2$ lone pair. CPK representations of several DOTAM metal complexes viewed down the rotation axis (Table 2) clearly show that the metal ions are entrapped in a molecular cage formed by the cyclen ring and the four acetamide pendant arms.^[42] Obviously, the conformational outcome of the *N*-substituents (i.e., extent of folding) is directly related to the ionic radius of the encapsulated cation. Indeed, the average metal–donor atom bond lengths increase as ion size grows. Larger metal ions, which are less well encapsulated in the macrocyclic cavity, get closer to the mean plane defined by the four amide oxygen atoms and the gap in the coordination sphere becomes more apparent. Accordingly, it might be anticipated that the tetraamine ring size also has a direct influence on the position of the donor atoms around the metal center. This is indeed the trend followed when the cyclen tether is replaced by a larger tetraazamacrocyclic. For example, with TETAM, the lead atom, which is located in between the four nitrogen and oxygen atom planes at almost identical distances ($\text{Pb} \cdots \text{N}_4 = 1.320$ Å, $\text{Pb} \cdots \text{O}_4 = 1.206$ Å), penetrates more deeply into the cavity than with DOTAM,^[14] while an intermediate situation is encountered in the case of the 13-membered analog TRITAM.^[61] As a con-

Table 2. Structural properties and CPK views down the axis passing through the centroids of the N₄ and O₄ planes of several DOTAM metal complexes.

	Zn ²⁺ [a]	Cd ²⁺ [a]	Ca ²⁺ [a]	Pb ²⁺ [b]
				
<i>r_i</i> [Å] ^[c]	0.74	1.10	1.12	1.29
Coordination number	6	8	8	8
M–N [Å]	2.25(4)	2.44(2)	2.59(3)	2.625(6)
M–O _{short} [Å]	2.10(6)	2.34(3)	2.396(1)	2.71(7)
M–O _{long} [Å]	3.18(17)	2.64(1)	2.418(8)	2.80(2)
M⋯N ₄ [Å]	0.94	1.26	1.51	1.55
M⋯O ₄ [Å]	1.54	1.32	1.09	0.96

[a] Ref.^[42]; atomic coordinates were retrieved from the Cambridge Structural Database. [b] This work. [c] Ionic radius; ref.^[35]

sequence, the acetamide arms can fold more easily over the cavity, leading to a more protective holodirected environment around the entrapped Pb²⁺ ion.

Hancock et al. suggested the use of a plot of the Pb–L bond lengths versus the L–Pb–Lp angles made between the Pb–L bonds and the hypothetical position of the lone pair (Lp) as a convenient means to detect a distortion or a gap in the coordination sphere and so to discern an active 6s² lone pair from an inactive one (Figure 6).^[44] Hemidirected geometries (i.e., stereoactive lone pair) were sought to produce plots evidencing large scattering and an increase in bond lengths when the L–Pb–Lp angle tends to zero.

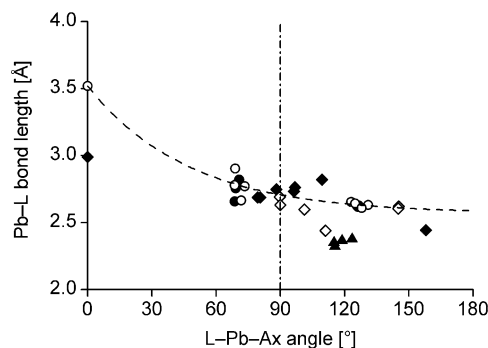


Figure 6. Plot of Pb–L bond lengths against the supposed L–Pb–Ax angle for [Pb(EDTA-N₄)]²⁺ (◇),^[62] [Pb(acac)₂] (▲),^[63] [Pb(18-crown-6)(SCN)₂] (◆),^[64] and [Pb(DOTAM)]²⁺ complexes (●, nitrate salt, this work; ○, perchlorate salt; the dashed line is drawn as an eye guide and is supposed to differentiate holodirected from hemidirected structures according to ref.^[44]). Atomic coordinates were retrieved from the Cambridge Structural Database.

The first issue with this approach is obviously related to the impossibility of precisely locating the position of the lone pair in a crystal structure. Hence, experimentalists have to presume stereoactivity and rely on their own judgment to localize the pair and estimate approximate values of the L–Pb–Lp angles. In the case of [Pb(DOTAM)]²⁺, a reasonable assumption was to localize the putative lone pair on

the rotation axis passing through the metal and the centroid of the four amine nitrogen atoms (Ct_N).

The second issue is the bias introduced in the original plot by Hancock et al.^[44] In addition to the eight almost uncorrelated data points corresponding to the directly bonded atoms, they took into account the point related to the water molecule located at 3.52 Å above the lead atom (O–Pb–Lp = 0°). Inclusion of this datum affords a graph with a decaying exponential shape (Figure 6), which was considered as a sufficient criterion sustaining stereochemical activity of the lone pair. However, if the latter point is excluded, the reverse conclusion could be reached. Therefore, the crystal structure of [Pb(DOTAM)](NO₃)₂·3.5H₂O determined in the present work offers a unique opportunity to test the validity of the approach proposed by Hancock et al. as the same complex was crystallized under different conditions and in the presence of a different counteranion. In the nitrate salt, the closest atom (O3_w belonging to a water molecule) sits 5.07 Å away from the Pb²⁺ ion (Ct_N–Pb–O3_w = 176.4), at a distance where any interaction with the lone pair can be ruled out. Thus, the scatter plot shown in Figure 6 definitively shows that the graphical approach to detect stereoactivity is meaningless if remote nonbonded atoms are considered.

Because donor atoms located opposite an active lone pair usually form much shorter bonds (L–Pb–Lp → 180°) than those closer to the equatorial plane (L–Pb–Lp → 90°),^[33] it seems more reasonable to consider only the directly bonded donor atoms to detect a distortion of the coordination polyhedron. Therefore, the structural descriptors of typical holo- and hemidirected lead(II) complexes are compared in Figure 6 with those of [Pb(DOTAM)]²⁺. These examples were chosen according to the facility to visually pinpoint the axis, noted Ax in Figure 7, along which the lone pair is supposed to be expanded.

The crystal structure of the complex formed with the hexadentate ligand *N,N,N',N'*-tetra(carbamoylmethyl)ethylenediamine (EDTA-N₄) reveals a hemidirected distribution of the donor atoms, while the lone pair is easily local-

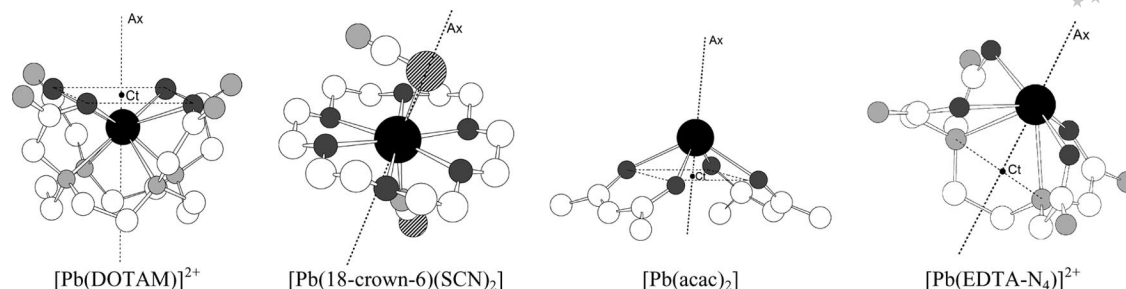


Figure 7. Definition of the Ax axis in several holo- and hemidirected lead(II) complexes. Atomic coordinates were retrieved from the Cambridge Structural Database.

ized because of the presence of a vacant hemisphere.^[62] This holds also for the bis(acetylacetonate) (acac) complex.^[63] However, a completely different situation is encountered when Pb^{2+} is bound to 18-crown-6.^[64] In the latter compound, the metal center is octacoordinated in the equatorial plane by the six oxygen atoms belonging to the macrocycle and by two thiocyanate anions on the axial positions. Because of the absence of a gap in the first coordination shell, it can thus be inferred that the structure is holodirected and that the $6s^2$ lone pair is stereochemically inactive.

For the clearly hemidirected complexes, the axis can be easily defined by the line passing through the Pb^{2+} ion and either the centroid of the O_4 plane for $[\text{Pb}(\text{acac})_2]$, or through the centroid of the N–N pair on the opposite side of the gap in the case of $[\text{Pb}(\text{EDTA-N}_4)]^{2+}$. For the holodirected $[\text{Pb}(\text{18-crown-6})(\text{SCN})_2]$ species, the axis was arbitrarily set along the S–Pb–S direction, as all donor atoms are symmetrically distributed in the coordination sphere. From a visual inspection of Figure 6, it becomes evident that there is no clear-cut difference between a holo- and a hemidirected arrangement. Nevertheless, it can be noticed that L–Pb–Ax angles for the hemidirected complexes are always higher than or equal to 90° , while they span the $0\text{--}180^\circ$ range for the holodirected $[\text{Pb}(\text{18-crown-6})(\text{SCN})_2]$ complex, indicating that donor atoms are located in both hemispheres around the metal center. It is noteworthy that data points pertaining to $[\text{Pb}(\text{DOTAM})]^{2+}$ are distributed on both sides of the 90° threshold, further suggesting that the lone pair most likely remains inactive both in the perchlorate as well as in the nitrate salts. If one can safely conclude that the graphical tool proposed by Hancock et al. is merely useless, a slight emergence of the $6s^2$ electron pair due to a moderate charge transfer to the 6p orbital cannot be definitively excluded.^[65]

Solution NMR Studies

As only broad ^1H and ^{13}C NMR signals could be observed at room temperature, suggesting dynamic behavior of $[\text{Pb}(\text{DOTAM})]^{2+}$ in D_2O or $[\text{D}_7]\text{DMF}$ solution, the spectra were assigned on the basis of two-dimensional $^1\text{H}\text{--}^1\text{H}$ COSY 45, $^1\text{H}\text{--}^1\text{H}$ NOESY, and $^1\text{H}\text{--}^{13}\text{C}$ HETCOR correlation maps recorded at 276 K in D_2O (see Supporting Information). By cooling the sample from 300 K down to 276 K, the three broad lines seen at room temperature be-

tween 2.5 and 4 ppm resolve into six multiplets assigned to the three sets of nonequivalent methylene protons, which could be easily paired with the help of a $^1\text{H}\text{--}^{13}\text{C}$ HETCOR experiment. These observations are consistent with a time-averaged C_{4v} symmetry in which all four acetamide arms are equivalent but where all the methylene protons become diastereotopic at temperatures close to the freezing point of D_2O . The large anisochrony affords strong evidence for the unidirectional orientation of the four amide substituents that differentiates both sides of the cyclen ring. A NOESY experiment enabled discrimination between the geminal cyclen protons directed towards the amide chains and those pointing away from them. Rapid exchange by a concerted flip-flop motion of each pair of geminal protons belonging to the twisted ethylenediamine chelate rings results in the coalescence above 300 K of each pair of diastereotopic signals. In order to visualize the N-terminal amide protons, a spectrum was also recorded in $[\text{D}_7]\text{DMF}$ that shows two singlets at $\delta = 8.32$ and 8.81 ppm. The large peak separation ($\Delta\delta = 0.5$ ppm) together with the C_{4v} symmetry suggests ligation of the carbonyl oxygen atoms to Pb^{2+} , as observed by X-ray crystallography.

Additional insight into the solution structure of the $[\text{Pb}(\text{DOTAM})]^{2+}$ cation was gained by means of ^{207}Pb NMR spectroscopy. Together with a nuclear spin of $1/2$, this isotope possesses a high receptivity, natural abundance (22.6%), and polarizability. It can thus be considered as a highly sensitive probe of the coordination environment, having chemical shifts spanning a range of more than 16000 ppm.^[62,66] The presence of a single resonance at $\delta = 1938$ ppm for a solution of about 5×10^{-2} M of $[\text{Pb}(\text{DOTAM})](\text{NO}_3)_2$ in D_2O confirms the presence of a single lead species and supports the coordination of lead(II) by four nitrogen and four neutral oxygen atoms in solution. Indeed, the observed chemical shift is in good agreement with the value reported by Claudio et al. for $[\text{Pb}(\text{EDTA-N}_4)]^{2+}$ ($\delta = 1764$ ppm), the tetraacetamide analog of EDTA.^[62] Ligation of two additional nitrogen atoms with respect to EDTA-N₄ might account for the 174-ppm downfield shift.

Whereas the ^1H and ^{207}Pb NMR spectra are in agreement with the eight-coordinate inverted square antiprismatic structure of $[\text{Pb}(\text{DOTAM})]^{2+}$ found in the crystal, VT NMR spectroscopic data indicate that the complex undergoes intramolecular interconversion between both enantiomeric forms. As already pointed out, helicity reversal of

the ethylenediamine chelate cycles interchanges the axial and equatorial positions of the diastereotopic methylene ring protons that become equivalent above 300 K. As stressed by Maumela et al.,^[42] this motion is concerted, with the inversion of configuration of the bound acetamide arms (Figure 3). The interconversion dynamics between the Δ -($\delta,\delta,\delta,\delta$) and Λ -($\lambda,\lambda,\lambda,\lambda$) enantiomers could be most conveniently followed by ^{13}C VT NMR studies. Experiments were carried out from 225 to 390 K in $[\text{D}_7]\text{DMF}$ on an instrument operating at 125 MHz (Figure 8).

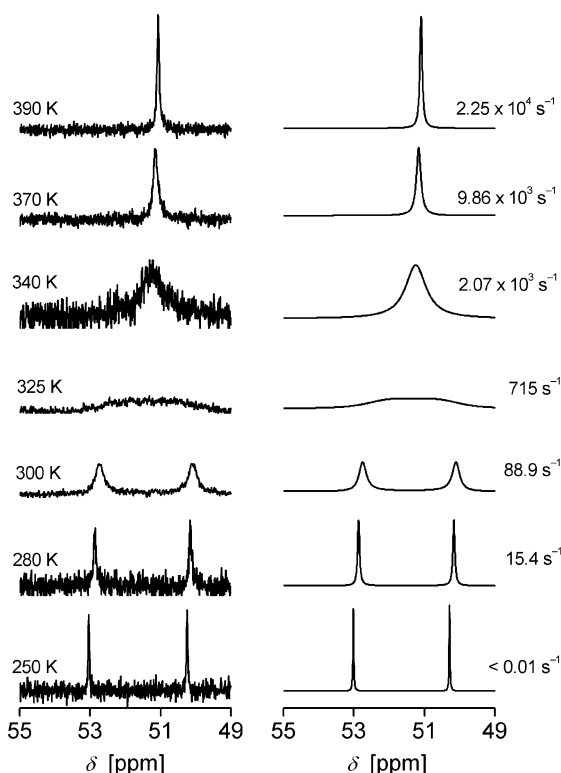


Figure 8. Variable-temperature 125-MHz ^{13}C NMR spectra of $[\text{Pb}(\text{DOTAM})]^{2+}$ in $[\text{D}_7]\text{DMF}$ showing the experimental (left) and simulated (right) resonances of the cyclen ring carbon atoms. Each experimental spectrum corresponds to the average of 1000 scans. Reported exchange rate constants (k) were derived by standard Lorentzian full line-shape analysis using the gNMR software.^[67]

While a single resonance is observed for the acetamide arms at any temperature, the eight cyclen carbon atoms divide into two groups of four equivalent nuclei below 320 K, as evidenced by the stack of spectra shown in Figure 8. Upon heating, a discrete spectral change is observed as both signals merge into a single peak with a coalesce temperature of $T_c = 322(1)$ K. Fast helicity interchange converting the Δ -($\delta,\delta,\delta,\delta$) enantiomer into its Λ -($\lambda,\lambda,\lambda,\lambda$) mirror image and vice versa renders all carbon atoms equivalent, while slow interconversion on the NMR timescale gives rise to a set of four atoms over which an arm is folded (Figure 3).^[68]

For each temperature, the associated first-order rate constant (k) was determined by full line-shape analysis using the gNMR software.^[67] The natural line width at half maximum was determined in the slow exchange regime. The in-

terconversion rate constants k were then fitted to the Eyring equation [Equation (1)] by nonlinear least-squares treatment to yield the activation parameters $\Delta H^\ddagger = 58.0(7)$ kJ mol $^{-1}$ and $\Delta S^\ddagger = -13(2)$ J mol $^{-1}$ K $^{-1}$.

$$k = \frac{k_B T}{h} \exp\left(-\frac{\Delta G^\ddagger}{RT}\right) = \frac{k_B T}{h} \exp\left(-\frac{\Delta H^\ddagger}{RT} + \frac{\Delta S^\ddagger}{R}\right) \quad (1)$$

Calculated activation free energy ($\Delta G^\ddagger = 62.2$ kJ mol $^{-1}$) and first-order exchange rate constant at 298 K ($k_{298} = 79$ s $^{-1}$) are in agreement with the values estimated by Maumela et al.^[42] from the coalescence temperature ($T_c = 305$ K, $\Delta G^\ddagger = 64.0$ kJ mol $^{-1}$) measured in D_2O . Activation enthalpies (ΔH^\ddagger) and entropies (ΔS^\ddagger) are of great value from a mechanistic standpoint.^[69] Low activation enthalpy and negative activation entropy are consistent with an intramolecular Bailar twist mechanism that proceeds by a concerted twist motion of the chelated arms about the C_4 axis via a tetragonal-prismatic transition state. Indeed, a dissociative mechanism involving Pb–L bond breaking would lead to a higher activation enthalpy and a positive activation entropy due to solvation. In turn, negative activation entropy is consistent with a tetragonal-prismatic transition state, which is more compact in solution than an inverted square antiprism.

Solution Equilibrium Studies

Cumulative stability constants reported hereafter as $\log \beta_{m,l,h}$ values are related to the general equilibrium (2), where m , l , and h refer to the stoichiometric coefficients of the three components, namely unhydrolyzed aquated metal ion (M), ligand (L), and hydronium ion (H), respectively. Charges have been omitted for clarity. Stepwise protonation constants K_{01i} are defined by the relation $\beta_{01h} = \prod K_{01i}$.



Because of the low solubility of free DOTAM in 0.1 M sodium perchlorate, the supporting electrolyte used for kinetic studies (vide infra), potentiometric measurements were carried out at 298.2 K in both 0.1 M sodium nitrate and potassium nitrate solutions (Table 3). The new data agree well with those reported by Brucher and co-workers in potassium-salt-containing solutions.^[70,71] As previously shown, the tetraamines bearing acetamide groups behave like weak diprotic bases between p[H] 2 and 11.

Overall, DOTAM [$\log \beta_{012} = 14.86(3)$] is more basic than TETAM [$\log \beta_{012} = 13.82(3)$] in spite of a lower K_{012} value. This increase in basicity is the sole result of the magnitude of difference in K_{011} of about 1.5 orders. The latter fact can be rationalized in terms of hydrogen-bonding interactions, as already pointed out in a previous work.^[15] Whereas the first protonation constant of DOTAM is typical for a tertiary amine not engaged in a hydrogen bond but bearing an electron-withdrawing group like an amide, involvement in an intramolecular hydrogen bond of each macrocyclic nitrogen atom of TETAM with one of the N-terminal amide protons hinders the protonation process and thus lowers the

Table 3. Protonation constants of DOTAM and TETAM, and stability constants of the corresponding lead(II) complexes at 298.2(2) K.

M		DOTAM	TETAM
H ⁺	log <i>K</i> ₀₁₁	8.91(2) ^[a]	7.44(2) ^[b]
		9.07 ^[c]	
		9.08(1) ^[d]	
		7.45(2) ^[e]	
		7.70(1) ^[f]	
		6.05 ^[c]	
	log <i>K</i> ₀₁₂	5.95(1) ^[a]	6.38(1) ^[b]
		6.44(1) ^[d]	
		5.92(1) ^[e]	
		6.21(1) ^[f]	
		14.86(3) ^[a]	
		15.12 ^[c]	
	log β ₀₁₂	6.44(1) ^[d]	13.82(2) ^[b]
		5.92(1) ^[e]	
		6.21(1) ^[f]	
		14.86(3) ^[a]	
		15.12 ^[c]	
		15.52 ^[d]	
Pb ²⁺	log β ₁₁₀	13.37(2) ^[e]	8.29(3) ^[b]
		13.91(1) ^[f]	
		>19 ^[f]	

[a] *I* = 0.1 M KNO₃; this work. [b] *I* = 0.1 M KNO₃ or NaClO₄; ref.^[15] [c] *I* = 0.1 M KNO₃; ref.^[70] [d] *I* = 1 M KCl; ref.^[71] [e] *I* = 0.1 M NaNO₃; this work. [f] *I* = 0.1 M NaNO₃; ref.^[42]

affinity towards H₃O⁺. According to the crystal structure of free DOTAM (Figure 1), only two out of the four tertiary nitrogen atoms are involved in hydrogen bonds. Therefore, one may tentatively conclude that the first protonation should occur on a non-hydrogen-bonded nitrogen atom.

Data collected in Table 3 also enable the medium effects on the proton affinity to be gauged. In contrast to TETAM,^[15] protonation constants of DOTAM determined in an aqueous sodium-salt-containing solution (0.1 M NaNO₃) are significantly lower than those measured in the presence of potassium nitrate at the same ionic strength. The influence of the supporting electrolyte on the protonation equilibria reflects the competition between alkaline and hydronium ion binding, the affinity for K⁺ being lower than for Na⁺, in agreement with the differences in ionic radii.^[35] Indeed, crystal structures of stable sodium complexes with DOTAM-like ligands bearing either secondary or tertiary amide pendant arms have been reported.^[72–74] Unexpectedly, there is a rather large discrepancy between the protonation constants determined in this work and those reported by Maumela et al. under identical conditions.^[42] In the present case, special care was taken to avoid systematic experimental errors by using a specifically designed high-alkalinity glass electrode in order to minimize the interference due to sodium ions.

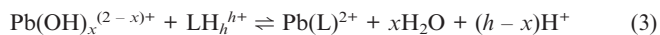
As DOTAM was known to form an extremely stable mononuclear lead(II) complex that withstands 0.5 M HCl, no further attempts were made to reevaluate the binding constant. The lower-limit estimate reported by Maumela et al. (log β₁₁₀ > 19)^[42] was considered in all speciation calculations. However, a spectrophotometric titration was performed in order to check the possible formation of [Pb(DOTAM)(OH)_{*h*}]^{(2–*h*)⁺} species under alkaline conditions. Provided a nonabsorbing counteranion such as ClO₄[–] is chosen, complex formation can be conveniently followed by UV absorption spectroscopy. Indeed, at p[H] values where

no hydrolysis occurs (about 2), the spectrum of an aqueous Pb(ClO₄)₂ solution is characterized by a strong absorption band (λ_{max} = 209 nm, ε_{max} = 11800 M^{–1} cm^{–1}) assigned to the spin-forbidden 6s² → 6sp transition. Spectral deconvolution by Gaussian line-shape fitting indicates that the envelope is composed of at least three components at 207.3, 205.3, and 212.2 nm. As an equimolar quantity of DOTAM is added to a 10^{–4} M Pb(ClO₄)₂ solution (*I* = 0.1 M NaClO₄), the aforementioned band disappears and is replaced by a new feature centered at 259 nm [ε_{max} = 9640(50) M^{–1} cm^{–1}] that remains unchanged from p[H] 3.5 to 10.5, excluding the putative formation of a hydroxido species.

Representative species distribution diagrams relevant to the kinetic studies are shown in Figure S11 as a function of p[H]. These diagrams are based on the protonation constants reported in Table 3 as well as the hydrolysis constants of lead(II).^[75] Accordingly, the mono- and diprotonated forms of DOTAM predominate in the p[H] range 4–7, although a small fraction of the free base is also present at the upper end. Lead(II) exists as a mixture of Pb²⁺ and the soluble hydroxido complex Pb(OH)⁺ if the solution is protected against CO₂ ingress, while the lead(II) complex is formed at more than 99.99% over the H₃O⁺ concentration range extending from 10^{–7} to 10^{–1} M.

Formation Kinetics

Taking all the relevant species into account, the overall complexation of lead(II) by DOTAM can be expressed by Equation (3), where L refers to DOTAM.



Depending on the experimental half-life, the time course of the reaction was monitored between p[H] 1 and 7 in weakly buffered solutions either by classical or stopped-flow single-wavelength spectrophotometry at 259 nm. Unfortunately, investigations at p[H] values higher than 7 were hampered by the occurrence of precipitates. The quantitative lead binding was treated as a pseudo-first-order process by degenerating the reaction order with respect to the ligand, concentrations after mixing being at least ten times larger than those of lead(II). Under such conditions, the reaction proceeds to completion in a single rate-limiting step with no more initial loss of spectrophotometric amplitude than that expected from the mixing time. The binding process was found to be of first order with respect to the entering metal, as the recorded signal could be fitted with an excellent statistical confidence to a single-exponential function by nonlinear least-squares.

The variation of the apparent pseudo-first-order rate constants (*k*_{obs}) with the analytical concentration of DOTAM exhibits a linear trend at any fixed p[H] value between 1 and 7 (plots and a table of the entire set of *k*_{obs} vs. [DOTAM]_{tot} data are available as Supporting Information). Linear regression analysis systematically returned intercepts that were not statistically different from zero according to

Student's *t*-test at the 95% probability level. Hence, the experimental k_{obs} values were adjusted to Equation (4), which supports the apparent rate law given by expression (5).

$$k_{\text{obs}} = k_f \times [\text{L}]_{\text{tot}} \quad (4)$$

$$v = \frac{d[\text{PbL}^{2+}]}{dt} = k_{\text{obs}} \times [\text{Pb}]_{\text{tot}} \quad (5)$$

The values of the second-order rate constants k_f listed in Table 4 were directly deduced from the slope of each regression line. It is worth noting that the change from formate to MES buffer around p[H] 4.5 did not significantly influence the reaction rates, as evidenced by the absence of discontinuity in the curve drawn in Figure 9. As the concentration of conjugated base at a similar p[H] value is obviously different for both buffers, this observation is a good hint for excluding a base-catalyzed binding mechanism.

Table 4. Formation rate constants (k_f) of $[\text{Pb}(\text{DOTAM})]^{2+}$.^[a]

p[H]	k_f [$\text{M}^{-1} \text{s}^{-1}$]	p[H]	$k_f \times 10^{-3}$ [$\text{M}^{-1} \text{s}^{-1}$]	p[H]	$k_f \times 10^{-3}$ [$\text{M}^{-1} \text{s}^{-1}$]
1.00	1.104(9)	4.43	3.97(3)	5.60	45.9(4)
1.59	4.71(1) ^[b]	4.45	4.20(4)	5.81	56.4(6)
1.60	4.94(5)	4.53	5.47(2)	6.19	92.2(6)
2.06	14.1(1)	4.64	7.71(4)	6.50	118.33(7)
3.00	135.6(8)	4.89	11.02(9)	6.88	132.6(9)
3.42	378(1)	5.21	18.69(8)	6.95	167(2)
4.02	1504(7)	5.37	29.6(2)		

[a] $[\text{Pb}]_{\text{tot}} = 2.015 \times 10^{-5} \text{ M}$; $I = 0.1 \text{ M}$ (H_2Na) ClO_4 ; $T = 298.2(2) \text{ K}$. p[H] was maintained constant within ± 0.01 unit by adding either HClO_4 ($\text{p[H]} = 1\text{--}2.06$), 0.025 M formate buffer ($\text{p[H]} = 3\text{--}4.45$), or 0.025 M MES buffer ($\text{p[H]} = 4.53\text{--}7$). [b] Reaction order degenerated with respect to lead(II) ($[\text{Pb}]_{\text{tot}} = 5.15 \times 10^{-4}\text{--}1.2 \times 10^{-2} \text{ M}$; $[\text{DOTAM}]_{\text{tot}} = 2.05 \times 10^{-5} \text{ M}$).

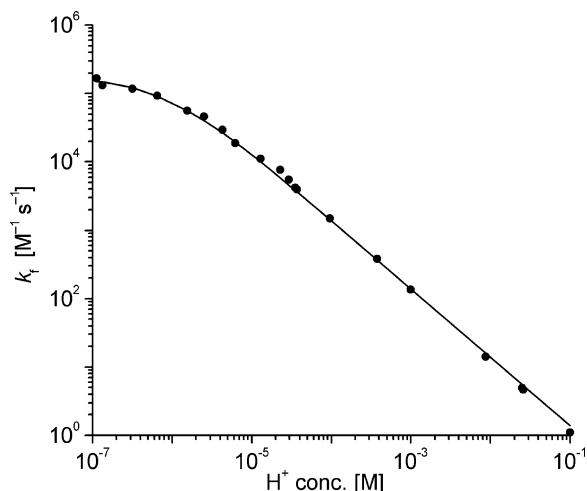
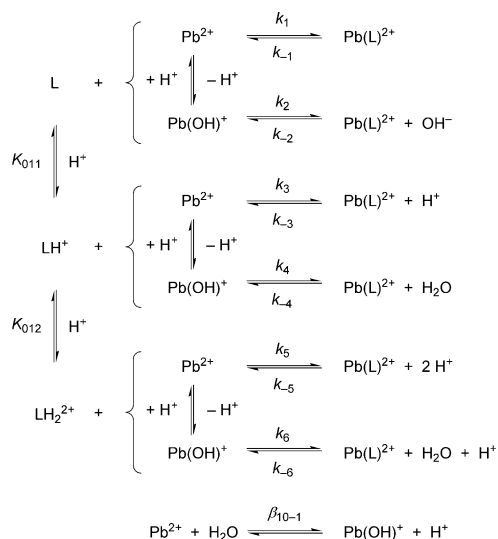


Figure 9. Variation of the rate constants k_f as a function of the proton concentration. $I = 0.1 \text{ M}$ (H_2Na) ClO_4 ; $T = 298.2(2) \text{ K}$.

Alternatively, the complex formation reaction was also monitored at $\text{p[H]} = 1.59$ but employing at least a 10-fold excess of lead perchlorate over ligand. Under such pseudo-first-order conditions, the monoexponential growth of the

optical density recorded at 259 nm confirmed that the reaction is also of first order with respect to the analytical DOTAM concentration. Moreover, k_{obs} values evidenced also a linear variation as a function of total lead concentration without any significant ordinate at the origin, the second-order rate constant being in excellent agreement with the value found by degenerating the reaction order with respect to the ligand (Table 4).

As seen in Figure 9, the second-order rate constants k_f are strongly pH-dependent. On a double-logarithmic scale, they decrease linearly with increasing free proton concentration over a wide range extending from p[H] 1 to ≈ 5.5 . The negative unitary slope of the straight line suggests an apparent reaction order of -1 with respect to the proton concentration. However, deviation from linearity occurring close to neutrality is a clear indication for a more complex mechanism that involves several protonated states of one or both reactants. According to the metal and ligand speciation diagrams (Figure S11), the reaction scheme should a priori take into account all possible pathways depicted in Scheme 2, where Pb^{2+} and its first hydrolysis product, $\text{Pb}(\text{OH})^+$, can react with either un-, mono-, or diprotonated DOTAM.



Scheme 2.

Integration of the rate law corresponding to Scheme 2 [Equation (6)] leads to expression (7), which relates k_f to the proton concentration and to the second-order intrinsic rate constants k_i ($i = 1\text{--}6$).^[15] According to the mass-balance equations, relation (7) also includes the hydrolysis constant of Pb^{2+} ion ($\beta_{10-1} = 10^{-7.32} \text{ M}$; $I = 0.1 \text{ M NaClO}_4$)^[75] and the cumulative protonation constants of DOTAM (β_{011} and β_{012} values given in Table 3 for 0.1 M NaNO_3). Because of the absence of any significant ordinate at the origin in the k_{obs} versus $[\text{L}]_{\text{tot}}$ plots [absence of a constant term in Equation (4)], reverse reactions in Scheme 2 can be neglected ($k_{-i} = 0$) in agreement with the extremely high stability of the formed lead complex.

$$v = \frac{d[\text{PbL}^{2+}]}{dt} = k_f[\text{L}]_{\text{tot}}[\text{Pb}]_{\text{tot}} = (k_1[\text{L}] + k_3[\text{LH}^+] + k_5[\text{LH}_2^{2+}][\text{Pb}^{2+}] + (k_2[\text{L}] + k_4[\text{LH}^+] + k_6[\text{LH}_2^{2+}][\text{Pb}(\text{OH})^+]) \quad (6)$$

$$k_f = \frac{k_2\beta_{10-1} + (k_1 + k_4\beta_{011}\beta_{10-1})[\text{H}^+] + (k_3\beta_{011} + k_6\beta_{012}\beta_{10-1})[\text{H}^+]^2 + k_5\beta_{012}[\text{H}^+]^3}{(1 + \beta_{011}[\text{H}^+] + \beta_{012}[\text{H}^+]^2)([\text{H}^+] + \beta_{10-1})} \quad (7)$$

The formation rate constants k_i ($i = 1-6$) of Equation (7) were adjusted to the experimental data by a weighted non-linear least-squares method,^[76] while the thermodynamic parameters β_{10-1} , β_{011} , and β_{012} were fixed. The employed weighting scheme [$\omega_i = (1/k_i)^2$], which assumes a constant relative error on k_f over the entire proton concentration range, approximately equalizes the contribution of each data point to the mean square sum. As this procedure is equivalent to a refinement on χ^2 , the expectation value for the goodness of fit (χ^2_{min}) is equal to the relative standard deviation of k_f values, which is close to 1% according to Table 4.

In the present case, only two of the six kinetic parameters could be determined, although proton ambiguity did not enable distinction of the two reaction schemes summarized in Table 5 that resulted in identical χ^2_{min} values ($\chi^2_{\text{min}} = 0.01655$). Over the entire explored $\text{p}[\text{H}]$ range, complex formation occurs primarily through the interaction of Pb^{2+} with the monoprotonated ligand species (k_3). If all the other reaction routes are neglected in the region where LH_2^{2+} and Pb^{2+} predominate ($\text{p}[\text{H}] < 5$), Equation (7) reduces to $k_f \approx (k_3/K_{012}) \times [\text{H}^+]^{-1}$, as experimentally suggested by Figure 9.

Table 5. Values of the second-order intrinsic formation rate constants of $[\text{Pb}(\text{DOTAM})]^{2+}$ adjusted by nonlinear regression analysis of the data shown in Figure 9 for both models affording the best fit.^[a]

Model	$k_1 \times 10^{-5}$ [M ⁻¹ s ⁻¹]	$k_3 \times 10^{-5}$ [M ⁻¹ s ⁻¹]	$k_4 \times 10^{-5}$ [M ⁻¹ s ⁻¹]
$\text{Pb}^{2+} + \text{L}$ and $\text{Pb}^{2+} + \text{LH}^+$	6.0(8)	1.19(4)	
$\text{Pb}^{2+} + \text{LH}^+$ and $\text{Pb}(\text{OH})^+ + \text{LH}^+$		1.19(4)	4.4(6)

[a] $I = 0.1 \text{ M}$ (H,Na) ClO_4 ; $T = 298.2(2) \text{ K}$.

However, this sole pathway does not account for the lower than expected second-order rate constants k_f for $\text{p}[\text{H}]$ values above about 5.5. Thus, a satisfactory fit was only obtained when the reaction of either Pb^{2+} with the free-base ligand (k_1) or $\text{Pb}(\text{OH})^+$ with the monoprotonated macrocycle (k_4) was also included in the model, in agreement with the species distribution diagrams shown in Figure S11. Although neither reaction scheme can be distinguished from a mathematical point of view, electrostatic considerations (vide infra) argue in favor of the first model in agreement with previous findings related to tetracarbamoyl derivatives of cyclam.^[15] Indeed, the rate enhancement factor of 5 experienced when Pb^{2+} reacts with the neutral ligand rather than the positively charged LH^+ form is in line with this assumption. On the other hand, interaction of $\text{Pb}(\text{OH})^+$ with LH^+ is also electrostatically more favorable than that of Pb^{2+} , while hydrolyzed metal ions are reputed to be more reactive, often by several orders of magnitude, than the fully aquated parent cation.^[77] Therefore, one

would expect a much higher than observed k_4/k_3 ratio, which does not exceed a factor of 3.7 in the present case.

Considering the main complex formation route, the reaction of Pb^{2+} with the monoprotonated form of DOTAM is much slower than expected for a dissociative Eigen–Wilkins mechanism.^[78] The refined k_3 value [$1.19(4) \times 10^5 \text{ M}^{-1} \text{ s}^{-1}$] is indeed three orders of magnitude lower than the $K_{\text{OS}} \times k_{\text{ex}}$ product ($\approx 3.6 \times 10^8 \text{ M}^{-1} \text{ s}^{-1}$), where K_{OS} stands for the stability constant of the $\{\text{Pb}(\text{H}_2\text{O})_x\}^{2+} \cdots \text{LH}^+$ outer-sphere complex and k_{ex} for the water-exchange rate constant for $[\text{Pb}(\text{H}_2\text{O})_x]^{2+}$ ($k_{\text{ex}} = 7.5 \times 10^9 \text{ s}^{-1}$ at 298 K).^[79] The K_{OS} value was estimated from the Fuoss theory by setting the closest approach distance between both constituents of the ion pair to $a = 5 \text{ \AA}$ ($K_{\text{OS}} = 0.048 \text{ M}^{-1}$).^[15] It is therefore concluded that the rate-limiting step takes place after the substitution of the first water molecule in the inner solvation shell, a situation that is commonly referred to as the so-called Eigen–Winkler mechanism.^[80] For comparison purposes, Table 6 summarizes the values of relevant intrinsic bimolecular rate constants (k_{LH}) reported in the literature pertaining to Pb^{2+} binding by monoprotonated cyclen, its tetrasubstituted acetate (DOTAH^{3-}) and acetamide (DOTAMH^+) derivatives, as well as TETAMH^+ . DOTAMH^+ is the less reactive compound within this series, the rate-limiting step being respectively 1.5×10^4 and 7 times slower than for DOTAH^{3-} and cyclenH^+ . The large dependency of the k_{LH} rate constants upon the nature of the entering ligand is a diagnostic feature for an Eigen–Winkler mechanism and thus provides further proof that such a process is operating for lead uptake by DOTAM.

Table 6. Values of the second-order intrinsic rate constants (k_{LH}) for the complexation of Pb^{2+} by monoprotonated macrocyclic ligands in buffered NaClO_4 solutions at 298.2 K.

Ligand		k_{LH} [M ⁻¹ s ⁻¹]	$k_{\text{LH}}/k_{\text{ex}}$ [M ⁻¹]	I [M]
Cyclen ^[a]	LH^+	$8.3(1) \times 10^5$	1.1×10^{-4}	0.2
DOTA ^[b]	LH^{3-}	$1.8(4) \times 10^9$	2.4×10^{-1}	0.1
DOTAM ^[c]	LH^+	$1.19(4) \times 10^5$	1.6×10^{-5}	0.1
TETAM ^[d]	LH^+	$1.36(5) \times 10^6$	1.8×10^{-4}	0.1

[a] Cyclen: 1,4,7,10-tetraazacyclododecane; ref.^[82] [b] DOTA: 1,4,7,10-tetrakis(carboxymethyl)-1,4,7,10-tetraazacyclododecane; ref.^[83] [c] This work. [d] TETAM: 1,4,8,11-tetrakis(carbamoylmethyl)-1,4,8,11-tetraazacyclotetradecane; ref.^[15]

In the case of unsubstituted tetraazamacrocycles, it has been shown that the rate-limiting step is often related to the formation of the second metal–nitrogen bond, while it is generally accepted that appending chelating groups on the ring structure accelerates the incorporation of metal cations in the molecular cavity.^[81] The 2200-fold larger rate constant reported in Table 6 for cyclenH^+ compared with that of DOTAH^{3-} can in large part be explained on the basis of

the Fuoss equation by taking into account the sole charge differences between the reacting ligand species, +1 ($K_{OS} = 0.048 \text{ M}^{-1}$) and -3 ($K_{OS} = 88.5 \text{ M}^{-1}$) respectively, as the ratio between the K_{OS} values approximates ≈ 1840 , assuming a closest approach distance of 5 Å.

Nevertheless, assistance of the acetate arms at the early stage of the lead(II) capture by DOTAH^{3-} is suggested by a saturation-type rate law, which is indicative of the rapid formation of an intermediate complex in equilibrium with the reactants prior to the rate-limiting step.^[83] Kasprzyk and Wilkins made similar observations when DOTAH^{3-} was opposed to an earth-alkaline (Ca^{2+} , Sr^{2+} , Ba^{2+}) or a divalent transition-metal cation (Ni^{2+} , Cu^{2+} , Zn^{2+}). They proposed that the metal ion was presumably bound to an acetate oxygen and a ring nitrogen atom in the intermediate monoprotonated complex.^[84] Further evidence for early participation of the acetate arms can be found in the prolific literature related to lanthanide(III) complexation by DOTA and related ligands that has been recently summarized by Moreau et al.^[85] The general picture that emerges is consistent with the rapid formation of a *N*-diprotonated intermediate in which all four acetate arms project in the same direction and are bound to the Ln^{3+} cation located above the O_4 plane. Five water molecules complete the coordination sphere. EXAFS data have shown that 60 h after the formation of the $[\text{Ln}(\text{DOTAH}_2)(\text{H}_2\text{O})_5]^+$ species, the lanthanide is still bound to the four carboxylic oxygen atoms but only three water molecules subsist in the solvation sphere while a concerted migration of both protons from the nitrogen to the bound oxygen atoms belonging to the same arms enables the first two Ln–N bonds to be established. This second $[\text{Ln}(\text{DOTAH}_2)(\text{H}_2\text{O})_3]^+$ intermediate can undergo fast deprotonation upon base addition with $\text{p}K_a$ values in the range of 2.5–2.7. Ultimate conversion of $[\text{Ln}(\text{DOTAH}_h)(\text{H}_2\text{O})_3]^{(h-1)+}$ ($h = 0-2$) into $[\text{Ln}(\text{DOTA})(\text{H}_2\text{O})]^-$ takes several additional weeks during which two water molecules are expelled from the coordination sphere while the Ln^{3+} cation penetrates into the molecular cavity and binds to the two last nitrogen atoms, affording the final species.^[86]

Although Pb^{2+} reacts by a factor of 7 slower with DOTAMH^+ than with cyclenH^+ , initial metal capture by the neutral acetamide dangling groups as described above cannot be ruled out a priori. One argument in favor of such a mechanism is provided by the crystallographic analysis of a diprotonated gadolinium tetraqua complex of DOTAM ,^[87] which has been considered as a thermodynamic key intermediate along the formation path leading to the final $[\text{Gd}(\text{DOTAM})(\text{H}_2\text{O})]^{3+}$ species.^[88] In $[\text{Gd}(\text{DOTAMH}_2)(\text{H}_2\text{O})_4]^{5+}$, the Gd^{3+} cation is surrounded outside the cavity by eight oxygen atoms according to a regular square antiprism. Projecting above the *trans*-diprotonated cyclen ring, the four acetamide arms provide a first set of oxygen atoms, while the four water molecules afford the second set. With one missing water molecule, this arrangement corresponds to that proposed for the first transient $[\text{Ln}(\text{DOTAH}_2)(\text{H}_2\text{O})_5]^+$ species. An overlay of both gadolinium DOTAM crystal structures was sought to give some

indication as to how the metal enters the cavity in order to interact with the tertiary amines upon deprotonation and release of three water molecules. Relocation of the carbamoyl arms results both in a more pronounced folding over the cyclen moiety and twisting around the C_4 symmetry axis but is also accompanied by a concerted puckering of each ethylenediamine fragment.

On the other hand, there are also a number of arguments against the rapid formation of such a protonated four-coordinate intermediate. In a recent work, Baranyai et al. have evidenced that the lanthanide(III) uptake by DOTAM follows a strict second-order process, having a rate law showing no saturation behavior, as found herein for lead(II).^[70] Performing kinetic studies between pH 4.7 and 5.8 with several Ln^{3+} cations (Ce^{3+} , Eu^{3+} , Gd^{3+} , Er^{3+} , Yb^{3+}), they realized also that unprotonated DOTAM was the reactive species and, most importantly, that the rate-determining step was not related to any deprotonation event. Two arguments were put forward to support this idea. ^1H NMR investigations enabled the rate law of deprotonation for free DOTAMH^+ to be established $\{k = 1.2(3) \times 10^3 + 5.3(5) \times 10^8 [\text{OH}^-]\}$. Accordingly, proton exchange was, by several orders of magnitude, faster than Ln^{3+} complexation over the explored pH range. In addition, the formation rate constants were independent at a given pH from the buffer concentration. Hence, they ruled out a formation mechanism similar to that outlined for $\text{DOTAH}_h^{(4-h)-}$ and suggested in turn that the rate-determining step was presumably associated with the second or third Ln^{3+} -amide bond formation.

The second objection against a DOTA-like mechanism is provided by the large basicity differences of an amide versus carboxylate oxygen atom, which makes a concerted proton transfer between the NH^+ and the coordinated oxygen atom highly unfavorable. Moreover, if such a mechanism operated, a multistep process would be anticipated: the first rapid rate-limiting binding step would be followed by much slower rearrangement events. This is in contrast with our findings. Moreover, the stability of such a putative transient species is expected to be much lower than that involving four negatively charged acetate donors ($\log K \approx 10^4$),^[83] because of the very weak basicity of amide oxygen atoms ($\text{p}K_a \approx -1$). Thus, its steady-state concentration should ipso facto be very low and this might explain why it was not possible to detect it under the present conditions.

Some time ago, we proposed that $[\text{Pb}(\text{TETAM})]^{2+}$ is formed according to a sequential arm-by-arm binding process with successive chelate ring closure.^[15] This assumption relies on several kinetic studies involving first-row transition metals and neutral cyclam derivatives bearing 2-hydroxyalkyl rests.^[89,90] Of particular relevance, Rahardjo and Wainwright showed that a minimum of two dangling *N*-hydroxyethyl chains appended to adjacent amines of 1,4-disubstituted cyclam are required to assist the metal ion capture by the oxygen atoms and speed up its insertion into the diprotonated macrocycle.^[91] Following this idea, $[\text{Pb}(\text{TETAM})]^{2+}$ formation could most probably be initiated by the fast replacement of two water molecules of the

fully aquated Pb^{2+} ion by the entering amide carbonyl oxygen atoms of TETAMH^+ and subsequent interaction with the tertiary amines bearing the amide groups, affording an O_2N_2 -bound intermediate.^[15,91] The driving force for such a sequential arm-by-arm binding process is the successive closure of five-membered chelate rings. Once the cation has been brought into the vicinity of the cyclam scaffold, the fifth bond formation could presumably involve a nitrogen atom located on the opposite side of the already bound amide arms. Deprotonation of the ammonium group and subsequent binding of the fourth tertiary amine was sought to occur in the final stage leading to the octacoordinate complex. As these ultimate steps most probably involve nitrogen inversion and significant conformational rearrangements that will invariably slow down the complexation process, we assumed that one of them was rate determining.

Considering that DOTAM and TETAM react with lead(II) according to the same rate law with second-order rate constants k_L and k_{LH} differing by a factor of about 17 and 11, respectively,^[15] this alternative mechanism might also apply to the 12-membered ligand. The late rate-determining step constitutes the major difference with the reaction scheme proposed by Baranyai et al.^[70] for $[\text{Ln}(\text{DOTAM})]^{3+}$ complex formation. Indeed, it is difficult to conceive that the size of the tetraazamacrocyclic scaffold would impact by a factor of ten or more the formation rates if the rate-determining step occurs at the early stage of the metal–ligand interaction (i.e., closure of the first chelate ring or third bond formation). In turn, the higher rigidity of a cyclen versus a cyclam moiety can reasonably account for the slower formation rates measured in the case of DOTAM if a late rate-determining step is postulated. However, a definitive assignment of the rate-determining step remains a challenging task.

Conclusions

Complementary instrumental techniques allowed us to update the physicochemical properties of the $\text{Pb}^{2+}/\text{DOTAM}$ system, both in the solid state as well as in solution, and to compare them with those found for the 14-membered cyclam analog TETAM. The structure of the free-base form of DOTAM has been determined both by X-ray crystallography and CPMA NMR spectroscopy. Two amide groups are engaged in intramolecular hydrogen bonds with the adjacent tertiary amines. New crystallographic data for the lead(II) complex with nitrate as counteranions support the N_4O_4 inverted square antiprismatic coordination environment provided by the ring nitrogen atoms and the amide substituents, while a careful analysis of the structure and comparison with literature data underscore the stereochemical inactivity of the $6s^2$ lone pair as a consequence of the holodirected arrangement of the donor atoms around the lead center.

Because of the four-blade propeller-like layout of the folded acetamide arms anchored on the cyclen scaffold, the $[\text{Pb}(\text{DOTAM})]^{2+}$ complex is chiral. While its integrity is

kept in aqueous solution, as evidenced by 2D NMR correlation spectroscopy, variable-temperature experiments performed in $[\text{D}_7]\text{DMF}$ enabled the interconversion mechanism of both C_{4v} -symmetric Δ -($\delta,\delta,\delta,\delta$) and Λ -($\lambda,\lambda,\lambda,\lambda$) enantiomers present in solution to be probed. The concerted helicity interchange of the five-membered acetamide and ethylenediamine chelate rings proceeds without decoordination through an intramolecular Bailar twist mechanism around the fourfold rotation axis with a tetragonal-prismatic transition state.

Advantage was taken of the high lead affinity of DOTAM, even under strongly acidic conditions, to study the formation kinetics in aqueous solution over a wide $\text{p}[\text{H}]$ range extending from 1 to 7. Similarly to the tetraacetamide-substituted cyclam analog TETAM, lead binding is first-order with respect to the entering metal and ligand and occurs in a single rate-limiting step. Analysis of the proton concentration dependence shown by the bimolecular rate constants indicated that the main reaction path involves Pb^{2+} and DOTAMH^+ , while above $\text{p}[\text{H}]$ 5.5 a second reaction has to be considered to account for the experimental data. Although proton ambiguity precludes definitive assignment, electrostatic considerations support the interaction of Pb^{2+} with the neutral free base form of the DOTAM as the most likely secondary pathway. As already found for TETAM, all the kinetic data are consistent with an Eigen–Winkler mechanism with a late rate-determining step. Complying to the binding mechanism proposed for cyclam derivatives bearing neutral hydroxy groups, an arm-by-arm chelation process leading to successive five-membered ring closure is favored over the fast formation of a PbO_4 intermediate in which all four carbonyl groups would be bound, followed by slow metal translocation and concerted proton transfer.

Experimental Section

General Considerations: Unless otherwise noted, all chemicals and starting materials were obtained commercially and used without further purification. DOTAM was prepared according to the procedure of Maumela et al.^[42] **Caution!** Although no problems were experienced in handling perchlorate compounds, these salts, when combined with organic ligands, are potentially explosive and should be manipulated with care and used only in very small quantities.

Synthesis of $[\text{Pb}(\text{DOTAM})](\text{NO}_3)_2 \cdot 3.5\text{H}_2\text{O}$: After dissolving equimolar amounts of lead nitrate (230 mg, 0.69 mmol) and DOTAM (278 mg, 0.69 mmol) in a methanol/water mixture (10:1 v/v) (20 mL), the solution was refluxed for 3 h and then concentrated to about 2 mL. Slow evaporation at room temperature afforded colorless prismatic crystals suitable for X-ray diffraction studies. The remaining crystals were filtered off, washed with a minimum amount of water and methanol, and dried. Yield: 225 mg, 41%. ^1H NMR (300 MHz, D_2O , $T = 300\text{ K}$): $\delta = 3.15$ (br. m, 16 H, NCH_2), 3.78 (br. s, 8 H, NCH_2CO) ppm. ^{13}C NMR (75 MHz, D_2O , $T = 300\text{ K}$): $\delta = 50.6$ (NCH_2), 52.9 (NCH_2), 56.3 (NCH_2CO), 175.7 (CH_2CO) ppm. ^{207}Pb NMR (104 MHz, D_2O , $T = 300\text{ K}$): $\delta = 1938$ ppm. IR (KBr pellets): $\tilde{\nu} \approx 3600$ (sh, ν_{OH} , H_2O), 3375 (br., $\nu_{\text{NH asym}}$), 3183 (br., $\nu_{\text{NH sym}}$), 2964 ($\nu_{\text{CH asym}}$), 2854 ($\nu_{\text{CH sym}}$), 1667

(ν_{CO}), 1615 (δ_{HNNH} and δ_{HOH}), 1350 (br., ν_{NO} , NO_3^-) cm^{-1} . MALDI-TOF MS: $m/z = 400.20$ [$\text{L}]^+$, 422.23 [$\text{L} + \text{Na} - \text{H}]^+$, 438.27 [$\text{L} + \text{K} - \text{H}]^+$, 606.62 [$\text{L} + \text{Pb} - 2\text{H}]^+$. $\text{C}_{16}\text{H}_{32}\text{N}_{10}\text{O}_{10}\text{Pb} \cdot 3.5\text{H}_2\text{O}$ (794.76); calcd. C 24.18, H 4.95, N 17.62, Pb 26.07; found C 24.51, H 4.78, N 17.50, Pb 25.83.

Physical and Spectroscopic Measurements: Microanalyses were performed on a Fisons EA 1108 CHNS instrument. The lead content was determined by inductively coupled plasma atomic emission spectroscopy (ICP-AES) using a Varian VISTA AX simultaneous spectrometer. MALDI-TOF mass spectra were obtained on a Bruker ProFLEX III spectrometer using dihydroxybenzoic acid as matrix. Infrared absorption spectra were measured as KBr pellets with an IFS 66v (Bruker) Fourier transform spectrophotometer from 4000 to 400 cm^{-1} with a 2 cm^{-1} resolution. Electronic absorption spectra were collected with a uniform data point interval of 1 nm with a Cary 50 (Varian) spectrophotometer equipped with a thermostatted cell holder connected to an RE106 (Lauda) water circulator. The optical path length of the quartz cell (Hellma) was 1 cm. $^1\text{H} \rightarrow ^{13}\text{C}$ and $^1\text{H} \rightarrow ^{15}\text{N}$ Cross-Polarization Magic Angle Spinning (CPMAS) NMR experiments were performed at room temperature on Avance II 300 and 400 spectrometers (Bruker) operating at $B_0 = 7.1$ and 9.4 T [Larmor frequencies $\nu_0 = 100.4$ MHz (^{13}C) and 30.4 MHz (^{15}N)], respectively. ^1H spin-lattice relaxation times (T_1) were evaluated with the inversion-recovery pulse sequence, indicating that a recycle delay of 60 s was necessary to avoid saturation for DOTAM. ^{13}C CPMAS NMR spectra were recorded with a 4-mm double-resonance MAS probe (Bruker) at a spinning frequency of 10 kHz, a ^1H $\pi/2$ pulse duration of 3.8 μs , a contact time of 2 ms, and a ^1H decoupling radio-frequency field of 65 kHz. Chemical shifts are relative to TMS. ^{15}N CPMAS NMR experiments were performed with a 7-mm double resonance MAS probe (Bruker) at a spinning frequency of 4 kHz, a ^1H $\pi/2$ pulse duration of 4.1 μs , a contact time of 5 ms, and a ^1H decoupling radio-frequency field of 65 kHz. Spectra were referenced indirectly by the ^{15}N signal of glycine ($\delta = -347.5$ ppm). The ^1H , proton-decoupled ^{13}C , and ^{207}Pb NMR solution spectra were recorded either with a Avance 300 or Avance DRX 500 spectrometer (Bruker) operating at 300.13 and 500.13 MHz, respectively. All chemical shifts are expressed in parts per million relative to the residual solvent peak^[92] or to an external standard [$\delta = 0$ ppm for a 1 M $\text{Pb}(\text{NO}_3)_2$ in D_2O containing 10^{-2} M HNO_3]. Variable-temperature ^{13}C NMR spectra were recorded with the Avance DRX 500 instrument in the 225–390 K range. The probe temperature, controlled by a BVT 3000 unit, was allowed to equilibrate for at least 10 min prior to final magnetic homogeneity optimization on the lock signal. Fluctuations at a given temperature were within ± 0.1 K.

X-ray Crystallography: Relevant experimental crystal data and refinement details are summarized in Table 7. Colorless and prismatic single-crystal specimens of both deprotonated DOTAM and $[\text{Pb}(\text{DOTAM})](\text{NO}_3)_2 \cdot 3.5\text{H}_2\text{O}$ complexes were selected for the X-ray diffraction experiments performed at $T = 110(2)$ K. Selected crystals were mounted with silicon grease on the tips of glass capillaries. While crystals of the free-base ligand were air-stable, those of the lead(II) complex underwent fast desolvation. Thus, several trials were necessary before a specimen, protected by a drop of silicon grease and quickly mounted on the goniometer head at low temperature, exhibited good diffraction quality. In order to minimize absorption effects in the case of the lead complex ($\mu = 5.967$ mm^{-1}), a parallelepiped-shaped crystal having approximately similar edge lengths along the three main directions ($0.13 \times 0.10 \times 0.10$ mm^3) was cut out within the mother liquor.

Table 7. Crystal data and structure refinement details for DOTAM (L) and its lead(II) complex.

Parameter	L	$[\text{Pb}(\text{L})](\text{NO}_3)_2 \cdot 3.5\text{H}_2\text{O}$
Empirical formula	$\text{C}_{16}\text{H}_{32}\text{N}_8\text{O}_4$	$\text{C}_{16}\text{H}_{39}\text{N}_{10}\text{O}_{13.5}\text{Pb}$
Formula mass [g mol^{-1}]	400.50	794.76
T [K]	110(2)	110(2)
Crystal system	monoclinic	monoclinic
Space group	$P2_1/c$	$P2_1/c$
a [Å]	5.9790(3)	9.2640(3)
b [Å]	17.8210(9)	26.4530(9)
c [Å]	9.4310(5)	12.2880(5)
β [°]	105.188(3)	107.916(2)
V [Å ³]	969.79(9)	2865.3(2)
Z	2	4
$d_{\text{calcd.}}$ [g cm^{-3}]	1.372	1.842
μ (Mo- K_α) [mm^{-1}]	0.101	5.967
Collected reflections	6322	12442
Unique reflections	3367 [$R_{\text{int}} = 0.0560$]	6398 [$R_{\text{int}} = 0.1030$]
Data/restraints/parameters	3367/0/177	6398/252/453
Goodness-of-fit on F^2 ^[a]	1.033	0.930
Final R indices	$R_1 = 0.0546$, $wR_2 = 0.0940$	$R_1 = 0.0621$, $wR_2 = 0.0906$
$[I > 2\sigma(I)]$ ^[a]	$R_1 = 0.1160$, $wR_2 = 0.1173$	$R_1 = 0.1861$, $wR_2 = 0.1158$
R indices (all data) ^[a]		
Largest diff. peak/hole [e Å^{-3}]	0.354/−0.281	1.491/−1.103

[a] Gof = $[\sum w(F_o^2 - F_c^2)^2 / (N_o - N_v)]^{1/2}$; $R_1 = \sum |F_o| - |F_c| / \sum |F_o|$; $wR_2 = \{\sum [w(F_o^2 - F_c^2)^2] / \sum [wF_o^4]\}^{1/2}$; $w = 1/[\sigma^2(F_o^2) + (AP)^2 + BP]$ where $P = (F_o^2 + 2F_c^2)/3$.

Diffraction data were collected on a Nonius KappaCCD diffractometer equipped with a nitrogen jet stream low-temperature system (Oxford Cryosystems). The X-ray source was graphite-mo-nochromated Mo- K_α radiation ($\mu = 0.71073$ Å) from a sealed tube. In both cases, lattice parameters were obtained by a least-squares fit to the optimized setting angles of the entire set of collected reflections. Intensity data were recorded as ϕ and ω scans with κ offsets. No significant intensity decay or temperature drift was observed during the data collections. Data were reduced by using DENZO software without applying absorption corrections; the missing absorption corrections were partially compensated for by the data scaling procedure in the data reduction.^[93] The structures were solved by direct methods using the SIR97 program.^[94] Refinements were carried out by full-matrix least-squares on F^2 using the SHELXL97 program^[95] and the complete set of reflections. Anisotropic thermal parameters were used for non-hydrogen atoms. In the crystal structure determination of DOTAM, all hydrogen atoms were located in the Fourier synthesis and their positional parameters were refined along with a global isotropic thermal factor. For $[\text{Pb}(\text{DOTAM})](\text{NO}_3)_2 \cdot 3.5\text{H}_2\text{O}$, all hydrogen atoms belonging to the ligand were located in the Fourier synthesis but those corresponding to the water molecules were not found. In that case, the located hydrogen atoms were placed at calculated positions using a riding model and refined with a global isotropic thermal factor.

CCDC-656319 and -656320 contain the supplementary crystallographic data for this paper. These data can be obtained free of charge from The Cambridge Crystallographic Data Centre via www.ccdc.cam.uk/data_request/cif.

Solution Preparations: All solutions were prepared with boiled and argon-saturated double-deionized high-purity water (18.2 MΩ cm) obtained from a Maxima (USF Elga) cartridge system designed for trace analysis. The carbonate-free KOH and NaOH solutions, prepared from Merck concentrates (Titrisol), were standardized by titrating against oven-dried (120 °C for 2 h) potassium hydrogen phthalate (Aldrich, 99.99%) and were stored under purified argon

using Ascariite II (Acros, 20–30 mesh) scrubbers in order to prevent absorption of carbon dioxide. The 0.1 M HNO_3 solution prepared from Merck concentrates (Titrisol) and the 0.1 M HClO_4 solution obtained by diluting analytical-grade concentrated perchloric acid (Fluka, 70%) were standardized against oven-dried (120 °C for 2 h) Tris buffer (Aldrich, 99.9%) using the equipment described below. Equivalent points were calculated by the second-derivative method. The concentration of the standardized solutions corresponded to the average of at least five replicates and was known with a relative precision of less than 0.15%. Ligand stock solutions for kinetic experiments were prepared by careful weighing with a Precisa 262SMA-FR balance (precision: ± 0.01 mg). The mother solution (0.0325 M) of $\text{Pb}(\text{ClO}_4)_2 \cdot 3\text{H}_2\text{O}$ (Across, 99%) was standardized with a 0.1 M $\text{Na}_2\text{H}_2\text{EDTA}$ solution (Titriplex III, Merck) using xylenol orange as an indicator.^[96]

Potentiometric Titrations: Acid-base titrations were carried out at constant ionic strength ($I = 0.1$ M) in a water-jacketed cell connected to a Lauda RE106 water circulator ensuring a constant temperature of 298.2(2) K. Magnetically stirred solutions were maintained under a low-pressure argon stream to exclude CO_2 from the headspace. Titrant aliquots were delivered through a polypropylene line from a calibrated automatic ABU901 (Radiometer-Tacussel) 10-mL piston buret. Volumes were corrected according to a linear calibration function obtained by weighing known quantities of water and by taking into account the buoyancy effect. Glass-bulb and reference electrodes were connected to a PHM240 ionometer (Radiometer-Tacussel) for recording the electromotive forces at ± 0.1 mV resolution. Both instruments were controlled by the Windows-based multitasking and interactive high-resolution titration software HRT Acid-Base Titration developed under the TestPoint environment by Mustin.^[97]

Depending upon the nature of the background electrolyte, two types of electrochemical cells were employed in order to limit interferences and alkaline errors. In KNO_3 solutions (0.1 M), a regular XG100 pH 0–12 electrode was used in conjunction with a XR110 KCl-saturated calomel reference electrode, whereas a XG200 high-alkalinity pH 0–14 electrode was selected in 0.1 M sodium-salt-containing solutions (NaNO_3 or NaClO_4 for the kinetic studies) together with a XR300 Ag/AgCl reference electrode filled with a saturated NaCl solution, all electrodes being purchased from Radiometer-Tacussel. The reference compartment was separated from the bulk of the solution by a sintered glass bridge filled with the appropriate 0.1 M supporting electrolyte solution. Prior to each experiment, the probe was calibrated to read hydronium ion concentrations ($\text{p[H]} = -\log[\text{H}_3\text{O}^+]$) by titrating standardized HNO_3 or HClO_4 (4.000 mL, 0.1 M) diluted in supporting electrolyte solution (25 mL) with standardized base (9.010 mL, 0.1 M) in 0.12-mL increments. Calibration data were processed according to a four-parameter extended Nernst equation, which takes into account liquid junction potentials in acidic and basic media.^[98] The ionic product of water at 298 K and $I = 0.1$ M was fixed to the literature value [$\text{p}K_w = 13.78(1)$ in all media].^[36]

The protonation constants of DOTAM were determined at a concentration level of about 4×10^{-3} M in the p[H] range 1.8–11.5. Following the experimental and processing procedures detailed elsewhere,^[98] each titration curve was analyzed individually by the weighted nonlinear least-squares refinement program Hyperquad 2000.^[99] In the last refinement step, the total amounts of ligand and initially added acid were also allowed to vary. The final values are reported as the arithmetic mean of at least three independent measurements together with their standard deviations, which were systematically higher than those derived for a single experiment

from the full variance/covariance matrix. Species distribution diagrams were computed with the help of Hyss software.^[100]

Kinetic Measurements: In all experiments, the ionic strength was maintained constant at 0.1 M by addition of the appropriate amount of $\text{NaClO}_4 \cdot \text{H}_2\text{O}$ (Merck), while p[H] values were adjusted with HClO_4 or NaOH. The spectroscopically silent and noncoordinating perchlorate anion was used throughout kinetic studies, as nitrate strongly absorbs light in the UV range. Because of the limited solubility of $[\text{Pb}(\text{DOTAM})](\text{ClO}_4)_2$ in water, the total lead concentration was kept below 5×10^{-5} M. Hence, only the ligand concentration could be varied to ensure pseudo-first-order conditions, albeit in a narrow range between 0.2 and 1×10^{-3} M because of the restricted solubility of the macrocycle in NaClO_4 media. During the course of the formation reaction, the p[H] was maintained constant within ± 0.02 units by addition of an adequate buffer. The nonabsorbing and very weakly coordinating 2-(*N*-morpholino)ethanesulfonate buffer (MES, $\text{p}K_a = 6.27$ at 298 K) was used for p[H] values between 4.5 and 7. Between 3 and 4.5, the p[H] was maintained constant with the help of a formic acid/formate buffer solution (0.025 M). For p[H] values around 4.5, the same results were obtained using either one or the other buffer. This observation is consistent with the noncoordinating properties of the formate ion. Below pH 3, dilute solutions of HClO_4 were used. In order to avoid ligand precipitation, the buffering substance was only introduced in the lead perchlorate solution, the final p[H] being adjusted with perchloric acid.

Formation rates were measured under pseudo-first-order conditions by using a SF-61 DX2 stopped-flow spectrophotometer from Hi-Tech Scientific. The drive syringes, mixing chamber, and optical cell were thermostatted at 298.2(2) K by water circulating from a RE106 (Lauda) constant-temperature bath. The reactants, maintained at this temperature for at least 15 min prior to injection, were mixed in less than 1.5 ms in a flow-through optical quartz cell of 1-cm path length. When complex formation was too slow to be monitored by stopped-flow spectrophotometry, spectral changes were detected using a Cary 50 (Varian) spectrophotometer. Reactants were then mixed together (2×1 mL) in a thermostatted quartz cell (Hellma) of 1-cm path length. Temperature was maintained constant at 298.2(2) K by water circulation through the double-walled cell holder connected to an RE106 (Lauda) bath.

The stopped-flow kinetic traces, recorded at the maximum of the UV absorption band assigned to the lead complex ($\lambda = 259$ nm), were averaged out of at least six replicates and then processed with the fitting routine implemented in the Kinet Asyst 2 (Hi-Tech Scientific) software. Alternatively, the general graphing program Origin 6.0 (Microcal)^[76] was used to analyze the single traces recorded with the Cary 50 instrument. Both packages enable a sum of one to three exponential functions to be fitted to the experimental curve by the Marquardt nonlinear least-squares algorithm. The goodness of fit was judged in terms of the statistical parameter χ^2 and by visual inspection of the residual plots. In all cases, a monoexponential absorbance increase was observed. The pseudo-first-order rate constants thus derived are included in the Supporting Information. Further linear regression and nonlinear least-squares calculations were performed with Origin 6.0.^[76] Standard deviations are reported throughout in parenthesis as the last significant digit.

Supporting Information (see footnote on the first page of this article): Bond lengths and angles for DOTAM; values of pseudo-first-order constants (k_{obs}) for the complexation of lead(II) by DOTAM; ^{13}C and ^{15}N CPMAS NMR spectra of DOTAM at 300 K; ^1H , ^{13}C , and ^{207}Pb NMR spectra of $[\text{Pb}(\text{DOTAM})](\text{NO}_3)_2 \cdot 3.5\text{H}_2\text{O}$ at 300 K; ^1H – ^1H COSY 45, ^1H – ^1H NOESY, and ^1H – ^{13}C HETCOR corre-

lation maps of $[\text{Pb}(\text{DOTAM})](\text{NO}_3)_2 \cdot 3.5\text{H}_2\text{O}$ at 276(1) K; Eyring plot for configuration inversion of $[\text{Pb}(\text{DOTAM})]^{2+}$ in $[\text{D}_7]\text{DMF}$; distribution diagrams of the lead(II) hydroxido and carbonato species in anaerobic conditions and under CO_2 , and of the protonated forms of DOTAM; and variation of the pseudo-first-order rate constants k_{obs} with the analytical concentration of lead(II) and DOTAM.

Acknowledgments

This work was carried out within the framework of the French governmental project "Réduire la teneur du plomb dans l'eau" (contract no. 99V0367 – Ministère Délégué à la Recherche et aux Nouvelles Technologies and Ministère de l'Équipement, des Transports et du Logement), and was also supported by the Agence Nationale de la Recherche (contract no. ANR-05-BLAN-0328-01), the Centre National de la Recherche Scientifique (CNRS), and the Conseil Régional de Bourgogne. F. C., A. B., and R. B. are grateful to the Ministère Délégué à la Recherche et aux Nouvelles Technologies, the Conseil Régional de Bourgogne, and the Commissariat à l'Énergie Atomique (CEA) for granting their Ph.D. scholarship.

- [1] A. E. Martell, R. D. Hancock, *Metal Complexes in Aqueous Solutions*, Plenum Press, New York, **1996**.
- [2] D. M. Roundhill, *Extraction of Metals from Soils and Waters*, Kluwer Academic/Plenum Publishers, New York, **2001**.
- [3] D. E. Reichert, J. S. Lewis, C. J. Anderson, *Coord. Chem. Rev.* **1999**, *184*, 3–66.
- [4] R. B. Martin in *Encyclopedia of Inorganic Chemistry* (Ed.: R. B. King), Wiley Interscience, Chichester, **1994**, vol. 2, p. 2195.
- [5] H. A. Godwin, *Curr. Opin. Chem. Biol.* **2001**, *5*, 223–227.
- [6] E. S. Claudio, H. A. Godwin, J. S. Magyar, *Prog. Inorg. Chem.* **2003**, *51*, 1–141.
- [7] N. N. Greenwood, A. Earnshaw, *Chemistry of the Elements*, Pergamon Press, Oxford, **1984**.
- [8] M. J. Warren, J. B. Cooper, S. P. Wood, P. M. Shoolingin-Jordan, *Trends Biochem. Sci.* **1998**, *23*, 217–221.
- [9] E. Sole, A. Ballabriga, C. Dominguez, *BioMetals* **1998**, *11*, 189–197.
- [10] C. M. L. S. Bouton, L. P. Frelin, C. E. Forde, H. A. Godwin, J. Pevsner, *J. Neurochem.* **2001**, *76*, 1724–1735.
- [11] C. Chenu, S. Colucci, M. Grano, P. Zigrino, R. Barattolo, G. Zamboni, N. Baldini, P. Vergnaud, P. D. Delmas, A. Z. Zalone, *J. Cell Biol.* **1994**, *127*, 1149–1158.
- [12] W. H. Liggett, J. B. Lian, J. S. Greenberger, J. Glowacki, *J. Cell. Biochem.* **1994**, *55*, 190–199.
- [13] T. L. Dowd, J. F. Rosen, L. Mints, C. M. Gundersen, *Biochim. Biophys. Acta* **2001**, *1535*, 153–163.
- [14] F. Cuenot, M. Meyer, A. Bucaille, R. Guillard, *J. Mol. Liq.* **2005**, *118*, 89–99.
- [15] F. Cuenot, M. Meyer, E. Espinosa, R. Guillard, *Inorg. Chem.* **2005**, *44*, 7895–7910.
- [16] K. Abu-Dari, F. E. Hahn, K. N. Raymond, *J. Am. Chem. Soc.* **1990**, *112*, 1519–1524.
- [17] K. Abu-Dari, T. B. Karpishin, K. N. Raymond, *Inorg. Chem.* **1993**, *32*, 3052–3055.
- [18] S. Rupprecht, S. J. Franklin, K. N. Raymond, *Inorg. Chim. Acta* **1995**, *235*, 185–194.
- [19] S. Rupprecht, K. Langemann, T. Lugger, J. M. McCormick, K. N. Raymond, *Inorg. Chim. Acta* **1996**, *243*, 79–90.
- [20] A. Pellissier, Y. Bretonnière, N. Chatterton, J. Pécourt, P. Delangle, M. Mazzanti, *Inorg. Chem.* **2007**, *46*, 3714–3725.
- [21] R. G. Pearson, *J. Am. Chem. Soc.* **1963**, *85*, 3533–3539.
- [22] R. G. Pearson, *Inorg. Chem.* **1988**, *27*, 734–740.
- [23] R. G. Pearson, *Inorg. Chim. Acta* **1995**, *240*, 93–98.
- [24] R. D. Hancock, H. Maumela, A. S. de Sousa, *Coord. Chem. Rev.* **1996**, *148*, 315–347.
- [25] D. Esteban-Gomez, C. Platas-Iglesias, T. Enriquez-Pérez, F. Avecilla, A. de Blas, T. Rodriguez-Blas, *Inorg. Chem.* **2006**, *45*, 5407–5416.
- [26] D. Esteban-Gomez, C. Platas-Iglesias, F. Avecilla, A. de Blas, T. Rodriguez-Blas, *Eur. J. Inorg. Chem.* **2007**, 1635–1643.
- [27] H. C. Freeman, G. N. Stevens, I. F. Taylor, *J. Chem. Soc. Chem. Commun.* **1974**, 366–367.
- [28] J. M. Morgan, *South. Med. J.* **1975**, *68*, 1001–1003.
- [29] M. Rivera, D. J. Levine, H. V. Aposhian, Q. Fernando, *Chem. Res. Toxicol.* **1991**, *4*, 107–114.
- [30] O. Andersen, *Chem. Rev.* **1999**, *99*, 2683–2710.
- [31] P. W. Wentz, *Chelation Therapy: Conventional Treatments*, Advance for Administrators of the Laboratory, Burlington, NC, **2000**. Report available at <http://laboratory-manager.advanceweb.com>.
- [32] R. J. Gillespie, I. Hargittai, *The VSEPR Model of Molecular Geometry*, Allyn and Bacon, Boston, **1991**.
- [33] L. Shimon-Livny, J. P. Glusker, C. W. Bock, *Inorg. Chem.* **1998**, *37*, 1853–1867.
- [34] R. D. Hancock, M. S. Shaikjee, S. M. Dobson, J. C. A. Boeyens, *Inorg. Chim. Acta* **1988**, *154*, 229–238.
- [35] R. D. Shannon, *Acta Crystallogr., Sect. A* **1976**, *32*, 751–767.
- [36] R. M. Smith, A. E. Martell, R. J. Motekaitis, *NIST Critically Selected Stability Constants of Metal Complexes Database*, release 6, NIST Standard Reference Data No. 46, Gaithersburg, MD, **2001**.
- [37] R. D. Hancock, A. E. Martell, *Chem. Rev.* **1989**, *89*, 1875–1914.
- [38] R. M. Izatt, J. S. Bradshaw, S. A. Nielsen, J. D. Lamb, J. J. Christensen, D. Sen, *Chem. Rev.* **1985**, *85*, 271–339.
- [39] R. M. Izatt, K. Pawlak, J. S. Bradshaw, R. L. Bruening, *Chem. Rev.* **1991**, *91*, 1721–2085.
- [40] R. M. Izatt, K. Pawlak, J. S. Bradshaw, R. L. Bruening, *Chem. Rev.* **1995**, *95*, 2529–2586.
- [41] C. Bazzicalupi, A. Bianchi, E. Berni, L. Calabi, C. Giorgi, P. Mariani, P. Losi, B. Valtancoli, *Inorg. Chim. Acta* **2002**, *329*, 93–99.
- [42] H. Maumela, R. D. Hancock, L. Carlton, J. H. Reibenspies, K. P. Wainwright, *J. Am. Chem. Soc.* **1995**, *117*, 6698–6707.
- [43] S. Brandès, F. Denat, M. Meyer, R. Guillard, *L'Act. Chim.* **2005**, *290–291*, 108–117.
- [44] R. D. Hancock, J. H. Reibenspies, H. Maumela, *Inorg. Chem.* **2004**, *43*, 2981–2987.
- [45] G. O. Lloyd, R. C. Luckay, *Acta Crystallogr., Sect. E* **2005**, *61*, o3405–o3407.
- [46] M. Meyer, V. Dahanoui-Gindrey, C. Lecomte, R. Guillard, *Coord. Chem. Rev.* **1998**, *178–180*, 1313–1405.
- [47] A. J. C. Wilson, E. Prince, *International Tables for Crystallography*, 2nd ed., Kluwer Academic Publishers, Dordrecht, **1999**, vol. C.
- [48] D. Quinonero, A. Frontera, M. Capo, P. Ballester, G. A. Suner, C. Garau, P. M. Deya, *New J. Chem.* **2001**, *25*, 259–261.
- [49] J. Dale, *Acta Chem. Scand.* **1973**, *27*, 1115–1129.
- [50] J. Dale, *Top. Stereochem.* **1976**, *9*, 199–270.
- [51] B. Bosnich, C. K. Poon, M. L. Tobe, *Inorg. Chem.* **1965**, *4*, 1102–1108.
- [52] L. Frémond, E. Espinosa, M. Meyer, F. Denat, R. Guillard, V. Huch, M. Veith, *New J. Chem.* **2000**, *24*, 959–966.
- [53] J. H. Reibenspies, *Acta Crystallogr., Sect. C* **1992**, *48*, 1717–1718.
- [54] K. Kumar, C. A. Chang, L. C. Francesconi, D. D. Dischino, M. F. Malley, J. Z. Gougoutas, M. F. Tweedle, *Inorg. Chem.* **1994**, *33*, 3567–3575.
- [55] T. Gyr, H. R. Mäcke, M. Hennig, *Angew. Chem. Int. Ed. Engl.* **1997**, *36*, 2786–2788.
- [56] S. Cavadini, S. Antonijevic, A. Lupulescu, G. Bodenhausen, *J. Magn. Reson.* **2006**, *182*, 168–172.
- [57] S. Hayashi, *Chem. Phys. Lett.* **1999**, *299*, 272–276.
- [58] K. P. Wainwright, *Coord. Chem. Rev.* **1997**, *166*, 35–90.

- [59] I. Lukes, J. Kotek, P. Vojtisek, P. Hermann, *Coord. Chem. Rev.* **2001**, 216–217, 287–312.
- [60] E. J. Corey, J. C. Bailar, *J. Am. Chem. Soc.* **1959**, 81, 2620–2629.
- [61] J. M. Lagrange, Ph.D. Thesis, Université de Bourgogne, Dijon, France, **2003**.
- [62] E. S. Claudio, M. A. Horst, C. E. Forde, C. L. Stern, K. Z. Matthew, H. A. Godwin, *Inorg. Chem.* **2000**, 39, 1391–1397.
- [63] K. Lyczko, J. Narbutt, B. Paluchowska, J. Maurin, I. Persson, *Dalton Trans.* **2006**, 3972–3976.
- [64] A. Y. Nazarenko, E. B. Rusanov, *Polyhedron* **1994**, 13, 2549–2553.
- [65] C. Gourlaouen, O. Parisel, *Angew. Chem. Int. Ed.* **2007**, 46, 553–556.
- [66] G. Oz, D. L. Pountney, I. M. Armitage, *Biochem. Cell Biol.* **1998**, 76, 223–234.
- [67] P. H. M. Budzelaar, *gNMR*, release 4.1, Cherwell Scientific Publishing, Oxford, **1995**.
- [68] S. F. Lincoln, *Coord. Chem. Rev.* **1997**, 166, 255–289.
- [69] M. Meyer, B. Kersting, R. E. Powers, K. N. Raymond, *Inorg. Chem.* **1997**, 36, 5179–5191.
- [70] Z. Baranyai, I. Banyai, E. Brücher, R. Kiraly, E. Terreno, *Eur. J. Inorg. Chem.* **2007**, 3639–3645.
- [71] A. Pasha, G. Tircso, E. T. Benyo, E. Brücher, A. D. Sherry, *Eur. J. Inorg. Chem.* **2007**, 4340–4349.
- [72] R. S. Dickins, J. A. K. Howard, J. M. Moloney, D. Parker, R. D. Peacock, G. Siligardi, *Chem. Commun.* **1997**, 1747–1748.
- [73] H. Tsukube, Y. Mizutani, S. Shinoda, M. Tadokoro, K. Hori, *Tetrahedron Lett.* **1997**, 38, 5021–5024.
- [74] R. S. Dickins, J. A. K. Howard, C. L. Maupin, J. M. Moloney, D. Parker, R. D. Peacock, J. P. Riehl, G. Siligardi, *New J. Chem.* **1998**, 22, 891–899.
- [75] F. Cuenot, Ph.D. Thesis, Université de Bourgogne, Dijon, France, **2004**.
- [76] *Origin 6.0*, Microcal Software Inc., Northampton, MA.
- [77] L. Helm, A. E. Merbach, *Chem. Rev.* **2005**, 105, 1923–1960.
- [78] M. Eigen, R. G. Wilkins, *Adv. Chem. Ser.* **1965**, 49, 55–67.
- [79] T. Yasunaga, S. Harada, *Bull. Chem. Soc. Jpn.* **1971**, 44, 848–850.
- [80] R. G. Wilkins, *Kinetics and Mechanism of Reactions of Transition Metal Complexes*, 2nd ed., VCH Publishers, Weinheim, **1991**.
- [81] H. Elias, *Coord. Chem. Rev.* **1999**, 187, 37–73.
- [82] M. Kodama, E. Kimura, *J. Chem. Soc. Dalton Trans.* **1977**, 2269–2276.
- [83] C. G. Pippin, T. J. McMurphy, M. W. Brechbiel, M. McDonald, R. Lambrecht, D. Milenic, M. Roselli, D. Colcher, O. A. Gansow, *Inorg. Chim. Acta* **1995**, 239, 43–51.
- [84] S. P. Kasprzyk, R. G. Wilkins, *Inorg. Chem.* **1982**, 21, 3349–3352.
- [85] J. Moreau, E. Guillon, J. C. Pierrard, J. Rimbault, M. Port, M. Aplincourt, *Chem. Eur. J.* **2004**, 10, 5218–5232.
- [86] F. Benetollo, G. Bombieri, L. Calabi, S. Aime, M. Botta, *Inorg. Chem.* **2003**, 42, 148–157.
- [87] P. A. Stenson, A. L. Thompson, D. Parker, *Dalton Trans.* **2006**, 3291–3293.
- [88] A. Barge, M. Botta, D. Parker, H. Puschmann, *Chem. Commun.* **2003**, 1386–1387.
- [89] B. Dey, J. H. Coates, P. A. Duckworth, S. F. Lincoln, K. P. Wainwright, *Inorg. Chim. Acta* **1993**, 214, 77–84.
- [90] R. W. Hay, M. M. Hassan, *Polyhedron* **1997**, 16, 2205–2211.
- [91] S. B. Rahardjo, K. P. Wainwright, *Inorg. Chim. Acta* **1997**, 255, 29–34.
- [92] H. E. Gottlieb, V. Kotlyar, A. Nudelman, *J. Org. Chem.* **1997**, 62, 7512–7515.
- [93] Z. Otwinowski, W. Minor, *Methods Enzymol.* **1997**, 276, 307–326.
- [94] A. Altomare, M. C. Burla, M. Camalli, G. L. Cascarano, C. Giacovazzo, A. Guagliardi, A. G. G. Moliterni, G. Polidori, R. Spagna, *J. Appl. Crystallogr.* **1999**, 32, 115–119.
- [95] G. M. Sheldrick, *SHELXL-97, Program for the Refinement of Crystal Structures*, University of Göttingen, Germany, **1997**.
- [96] *Méthodes d'analyses complexométriques avec les Titriplex*, E. Merck, Darmstadt, **1990**.
- [97] G. Naja, C. Mustin, B. Volesky, J. Berthelin, *Water Res.* **2005**, 39, 579–588.
- [98] M. Meyer, L. Frémond, A. Tabard, E. Espinosa, G. Y. Vollmer, R. Guillard, Y. Dory, *New J. Chem.* **2005**, 29, 99–108.
- [99] P. Gans, A. Sabatini, A. Vacca, *Talanta* **1996**, 43, 1739–1753.
- [100] L. Alderighi, P. Gans, A. Ienco, D. Peters, A. Sabatini, A. Vacca, *Coord. Chem. Rev.* **1999**, 184, 311–318.

Received: August 2, 2007

Published Online: November 7, 2007